Improvement of GRCop-84 Through the Addition of Zirconium

David L. Ellis and Bradley A. Lerch
Glenn Research Center, Cleveland, Ohio

NASA STI Program . . . in Profile

Since its founding, NASA has been dedicated to the advancement of aeronautics and space science. The NASA Scientific and Technical Information (STI) program plays a key part in helping NASA maintain this important role.

The NASA STI Program operates under the auspices of the Agency Chief Information Officer. It collects, organizes, provides for archiving, and disseminates NASA's STI. The NASA STI program provides access to the NASA Aeronautics and Space Database and its public interface, the NASA Technical Reports Server, thus providing one of the largest collections of aeronautical and space science STI in the world. Results are published in both non-NASA channels and by NASA in the NASA STI Report Series, which includes the following report types:

- TECHNICAL PUBLICATION. Reports of completed research or a major significant phase of research that present the results of NASA programs and include extensive data or theoretical analysis. Includes compilations of significant scientific and technical data and information deemed to be of continuing reference value. NASA counterpart of peer-reviewed formal professional papers but has less stringent limitations on manuscript length and extent of graphic presentations.

- TECHNICAL MEMORANDUM. Scientific and technical findings that are preliminary or of specialized interest, e.g., quick release reports, working papers, and bibliographies that contain minimal annotation. Does not contain extensive analysis.

- CONTRACTOR REPORT. Scientific and technical findings by NASA-sponsored contractors and grantees.

- CONFERENCE PUBLICATION. Collected papers from scientific and technical conferences, symposia, seminars, or other meetings sponsored or cosponsored by NASA.

- SPECIAL PUBLICATION. Scientific, technical, or historical information from NASA programs, projects, and missions, often concerned with subjects having substantial public interest.

- TECHNICAL TRANSLATION. English-language translations of foreign scientific and technical material pertinent to NASA's mission.

Specialized services also include creating custom thesauri, building customized databases, organizing and publishing research results.

For more information about the NASA STI program, see the following:

- Access the NASA STI program home page at *http://www.sti.nasa.gov*

- E-mail your question via the Internet to *help@sti.nasa.gov*

- Fax your question to the NASA STI Help Desk at 443–757–5803

- Telephone the NASA STI Help Desk at 443–757–5802

- Write to:
  NASA Center for AeroSpace Information (CASI)
  7115 Standard Drive
  Hanover, MD 21076–1320

Improvement of GRCop-84 Through the Addition of Zirconium

David L. Ellis and Bradley A. Lerch
Glenn Research Center, Cleveland, Ohio

Acknowledgments

Level of Review: This material has been technically reviewed by technical management.

Available from

Improvement of GRCop-84 Through the Addition of Zirconium

David L. Ellis and Bradley A. Lerch
National Aeronautics and Space Administration
Glenn Research Center
Cleveland, Ohio 44135

Summary

GRCop-84 (Cu-8 at.% Cr-4 at.% Nb) has excellent strength, creep resistance, low cycle fatigue (LCF) life and stability at elevated temperatures. It suffers in comparison to many commercially available precipitation-strengthened alloys below 500 °C (932 °F). It was observed that the addition of Zr consistently improved the mechanical properties of Cu-based alloys especially below 500 °C. In an effort to improve the low-temperature properties of GRCop-84, 0.35 wt% Zr was added to the alloy. Limited tensile, creep, and LCF testing was conducted to determine if improvements occur. The results showed some dramatic increases in the tensile and creep properties at the conditions tested with the probability of additional improvements being possible through cold working. LCF testing at room temperature did not show an improvement, but improvements might occur at elevated temperatures.

1.0   Introduction

GRCop-84 (Cu-8 at.% Cr-4 at.% Nb) is a NASA-developed alloy designed for use in rocket engine combustion chamber liners and other high-temperature, high-heat-flux applications. The microstructure consists of Cr_2Nb particles in a nearly pure Cu matrix. Available literature exists that contains the mechanical properties of several Cu-based alloys of approximately equal composition with and without the addition of small amounts of Zr (0.1 to 1 wt%) (Refs. 1 to 5). Examples include Cu/Cu-Zr and Cu-Cr/Cu-Cr-Zr. As is shown in Figure 1, the addition of small amounts of Zr, normally accompanied by cold work, increases the low cycle fatigue (LCF) life twofold to thirtyfold. Similar increases have been observed for other mechanical properties of interest, such as tensile strength and creep life. Prior work has indicated that the addition of Zr results in a Cu_xZr precipitate, with x being 4, 4.5, or 5 (Ref. 6). Even in the presence of large amounts of Cr, which could form a Cr_2Zr phase, the Cu_xZr phase is favored (Refs. 7 to 9). On the basis of these observations, the authors hypothesized that adding Zr to GRCop-84 would result in the formation of a third phase that could strengthen the alloy and improve its properties further.

Only 0.17 wt% Zr can be dissolved into solid Cu at the eutectic temperature of 972 °C (1781 °F), with the solubility decreasing rapidly at lower temperatures (Ref. 6), but the available literature indicates that only small amounts of Zr are required to result in large changes in mechanical properties. Commercially available Cu-Zr contains only 0.15 wt% Zr, yet it is much stronger than pure Cu following heat treatment (Ref. 2). It was decided to attempt to add 0.35 wt% Zr to GRCop-84. The level was selected on the basis of the apparent need for at least 0.15 wt% Zr for effective strengthening, the Cu-Zr phase diagram, and an expectation that some Zr would be lost through vaporization during the melting process.

A Cu_xZr phase is precipitated in two steps. First the Zr is placed into solid solution using a high-temperature-solutioning heat treatment step. Typically this is carried out between 900 and 950 °C (1652 and 1742 °F). The temperature is limited to 972 °C (1782 °F) by the Cu-rich Cu-Zr eutectic (Ref. 6). Higher temperatures carry the risk of incipient melting. A water quench is used to prevent precipitation of Cu_xZr precipitates during cooling to room temperature. An aging heat treatment at a moderate temperature range, such as 425 to 525 °C (800 to 975 °F), is used to precipitate fine Cu_xZr particles from the Cu-Zr supersaturated solid solution. The fine precipitates strengthen the alloys. They also retard recovery, recrystallization, and grain growth, so the benefits of cold work are retained at higher temperatures (Ref. 10).
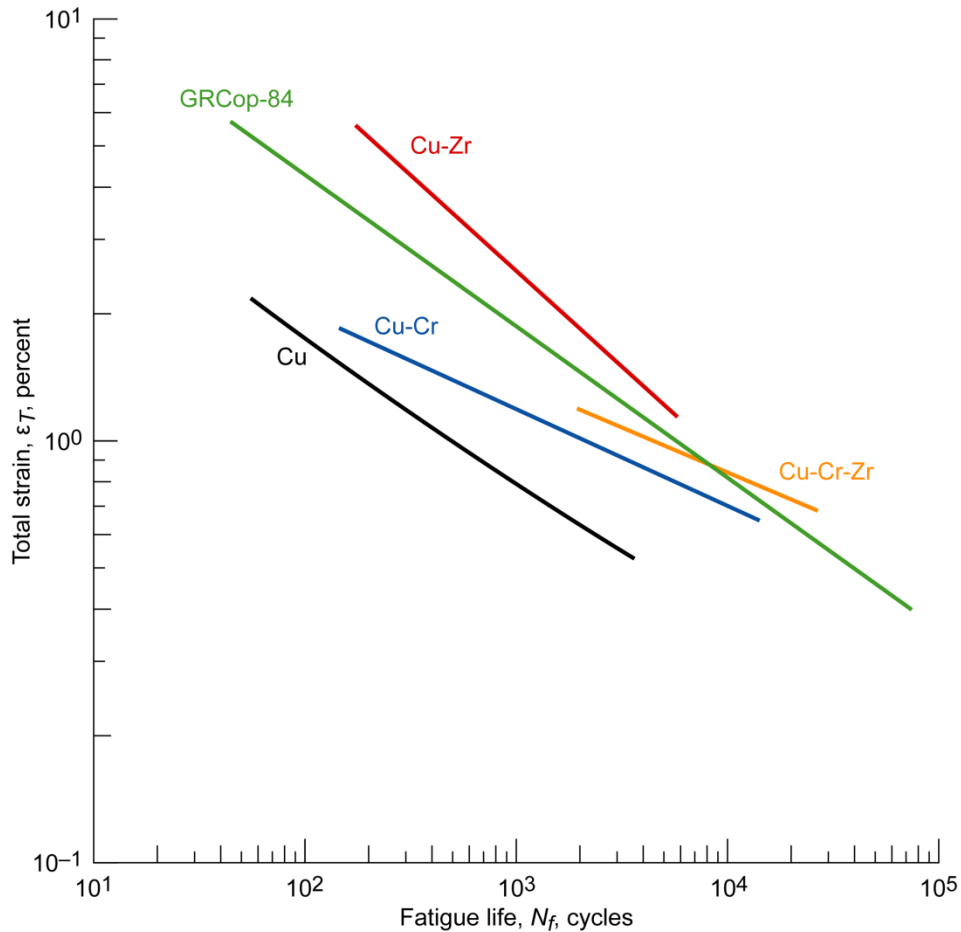
Figure 1.—Beneficial effects of small Zr additions on low cycle fatigue (Refs. 1 to 5).

This work was conducted under NASA Glenn Research Center's Director's Discretionary Fund program. Two goals were established in this work to improve the mechanical properties of GRCop-84. The first was a 15-percent increase in the yield strength between room temperature and 400 °C (752 °F). The second was an increase of 50 percent in the LCF life of the alloy. If these were successful, additional properties, such as conductivity, would be measured and a preliminary database would be established.

No specific application was targeted by this work, but if the low- and middle-temperature mechanical properties could be improved, the alloy would become competitive with the Cu-Cr, Cu-Zr, Cu-Cr-Zr, and Cu-Be alloys. These alloys and others are used in a wide variety of applications, including terminals and connectors for electrical, electronic, and automotive applications; springs for relay contacts and switchgear; integrated circuit leadframes; busbars; rotor bars; armatures; commutators; spot welding electrodes; heavy electrical switchgear; molds for continuous and static casting; and tuyéres for steelmaking blast furnaces (Ref. 11). In addition, improved mechanical properties would be beneficial for rocket engine combustion chamber liners, the primary application for GRCop-84.

It was decided to first determine the best solutioning temperature. The alloy was to be tested in the as-received condition, the aged condition, the cold-worked then aged condition, and the aged then cold-worked condition. The last two conditions were selected on the basis of the processing typical of Cu-Zr alloys (Ref. 6). Because funding was terminated early, only the as-received and aged conditions were tested. The aging temperature and time would be determined from the tensile tests, but the first attempts would use the same conditions typically used to process Cu-0.15 wt% Zr (Refs. 11 and 12).

2.0   Experimental Procedure

Under Glenn's Director's Discretionary Fund task, the tensile, creep, and LCF properties were surveyed to determine if the addition of Zr improved GRCop-84 properties. The microstructure was also examined in the as-received and heat-treated conditions to determine what changes could be observed. Because the program was terminated early, the complete test matrix, which included cold working the material to a full hard state, was not completed. Only material in the as-extruded and aged conditions was examined prior to completion of the current work. Microstructural characterization also was limited.

2.1   Alloy Design and Production

The addition of Zr to Cu results in the formation of an intermetallic Cu_xZr phase. Various reports in the literature have indicated that the value of x can be 4 (Ref. 13), 4.5 (Ref. 14), or 5 (Ref. 15) for Cu-rich alloys. Some early work even indicated that x could be as low as 3 (Ref. 16). The accepted value of x in a binary Cu-Zr alloy is 4.5 (Ref. 6), but in the ternary Cu-Cr-Zr alloy, x was observed to be 5 (Ref. 9). The composition and structure of the precipitates will have an effect on the volume fraction and, hence, the total strengthening that can be achieved. The exact composition was not as important for this survey as was proving the ability to produce precipitates that result in significant improvements in the mechanical properties.

So that the target composition of the alloy could be determined, it was assumed that 100 percent of the Zr would be used in the formation of Cu_xZr precipitates, and x was set to 5 on the basis of the Cu-Cr-Zr experience. The amount of Cr and Nb were adjusted slightly downward from the GRCop-84 nominal composition to reflect the change in overall composition and to keep the volume fraction of Cr_2Nb precipitates constant at 14 vol%. In practice the differences were negligible and fell well within normal variability observed in past GRCop-84 production runs. The target composition, given in Table I, retained the slight excess of Cr used to control hydrogen embrittlement in GRCop-84. For reference, the nominal composition of GRCop-84 also is given in Table I. The Cu-Cr-Nb-Zr alloy was designated GRCop-84Z to indicate that it was GRCop-84 modified by the addition of Zr.

TABLE I.—GRCop-84 AND GRCop-84Z COMPOSITIONS

Composition, wt% (at.%)						
Element						
Cr	Nb	Fe	Hf	O	Zr	Cu
GRCop-84Z target composition						
6.65 (8.17)	5.81 (3.99)	<0.0050	<0.0020	<0.0400	0.35 (0.25)	Balance
GRCop-84 nominal composition						
6.69 (8.20)	5.83 (4.00)	<0.0050	(a)	<0.0400	(a)	Balance

aNot applicable.

Prior experiences with Cu-Cr-Nb (Ref. 17) and Cu-Cr-Zr (Ref. 9) indicated that conventional casting techniques produce very coarse precipitates not at all suited for strengthening an alloy. A finer microstructure is required. As with GRCop-84, commercial argon gas atomization was selected to refine the microstructure. Atomization was done at Crucible Research in Pittsburgh, Pennsylvania—the same company responsible for producing GRCop-84 powder. The same production methods and procedures were used as for GRCop-84 to minimize differences that would result from processing changes.

The same high-purity (minimum 99.99 wt%) elemental melt stock that was used for GRCop-84 was used for the production of GRCop-84Z except Zr was added. A 99.9 wt% Zr+Hf (maximum 2 wt% Hf) melt stock was used for the Zr addition. Approximately 23 kg (50 lb) of –140 mesh (<106-μm-diameter) powder was produced. The powder was produced, sieved, and stored under Ar to prevent oxidation. A small representative sample was sieved to produce a size distribution. The remaining powder was placed

into a 15.2-cm- (6-in.-) diameter 1018 carbon steel can and evacuated. Once the argon was removed, the fill tube was crimped and welded shut.

The powder was consolidated using direct hot extrusion at HC Starck in Coldwater, Michigan. The extrusion parameters and practices for GRCop-84 were again used to minimize processing effects. The extrusion billet was extruded into a rectangular bar with a 3.8- by 6.4-cm (1.5- by 2.5-in.) cross section. The total reduction in area was 7.5. On the basis of prior experience with GRCop-84, the authors expected that this would result in complete consolidation of the powder.

A Varian, Inc., Vista-PRO Inductively Coupled Plasma (ICP) Atomic Emission Spectrometer was used for chemical analysis of the major elements and Fe. The unit also was used to search for trace contaminants. Oxygen was analyzed with a LECO Corporation TC–436 Nitrogen-Oxygen Analyzer. ATI Powder Metals[1] analyzed the starting powder using ICP atomic emission spectroscopy and a LECO nitrogen-oxygen analyzer. Both units were comparable to Glenn's analytical instruments.

2.2   Heat Treatment Development

Because the extrusion billet was held at elevated temperature for extended periods of time, any Zr that was in solution would probably precipitate prior to extrusion. This meant that a two-step heat treatment would be required to solution and precipitate the Zr.

All heat treatments were done at Glenn. Samples approximately 3.8 by 6.4 by 2.5 cm (1.5 by 2.5 by 1 in.) were cut from the nose of the extruded bar. One specimen each was heat treated at 900, 925, and 950 °C (1652, 1697, and 1742 °F) for 30 min and water quenched (WQ). Higher temperatures would have been desirable, but the Cu-Zr phase diagram indicated the possibility of partial melting if the temperature was raised further (Ref. 6). The hardnesses of the samples were measured before and after heat treatment to determine if the hardness decreased, indicating that Zr was going into solution. A portion of the heat-treated material was also examined metallographically to determine if the Cu_xZr phase could be observed and seen to decrease relative to the as-received material.

The hardness was measured using a Newage Testing Instruments ME–1 hardness tester. The unit was calibrated prior to testing the samples using the procedure and standard calibration blocks supplied by New Age. Calibration blocks for Rockwell B scale hardnesses of 65, 75, and 85 HR_B were used for the calibration since they were expected to cover the entire range of sample hardnesses. A minimum of five measurements were taken to determine the average hardness of the material in the as-extruded, solution-heat-treated, and aged conditions.

The results of the solutioning heat treatment, which are detailed in Section 3, led to the selection of 950 °C as the solutioning temperature. Cu-Zr alloys are typically aged at 425 °C (800 °F) if they have been cold worked prior to aging and at 525 °C (975 °F) if they have not been cold worked (Refs. 2, 11, and 12). These temperatures plus 475 °C (890 °F) were selected for the current material. Two aging times were selected for each temperature as well to determine if the alloy underwent slow or rapid precipitation kinetics or would be prone to overaging at reasonable aging times. For 425 and 475 °C, times of 30 and 90 min were selected, and for 525 °C, times of 30 and 60 min were selected. All samples were air cooled (AC). As will be explained in Section 3, the maximum time for the 525 °C age was extended to 90 min because the precipitation and growth of the Cu_xZr precipitates was sluggish and because it was desired to have only two aging times.

2.3   Phase Identification

X-ray diffraction (XRD) with a Bruker D8 ADVANCE XRD unit with a Cu x-ray tube and K-α radiation was used to determine the major phases present in as-extruded GRCop-84Z. Multiple slow scans were conducted to determine which phases were present, and angles that corresponded to possible Cu-Zr phases received additional scans. Only the as-extruded bar was tested.

---

[1]ATI Powder Metals was formerly Crucible Research, Pittsburgh, PA.
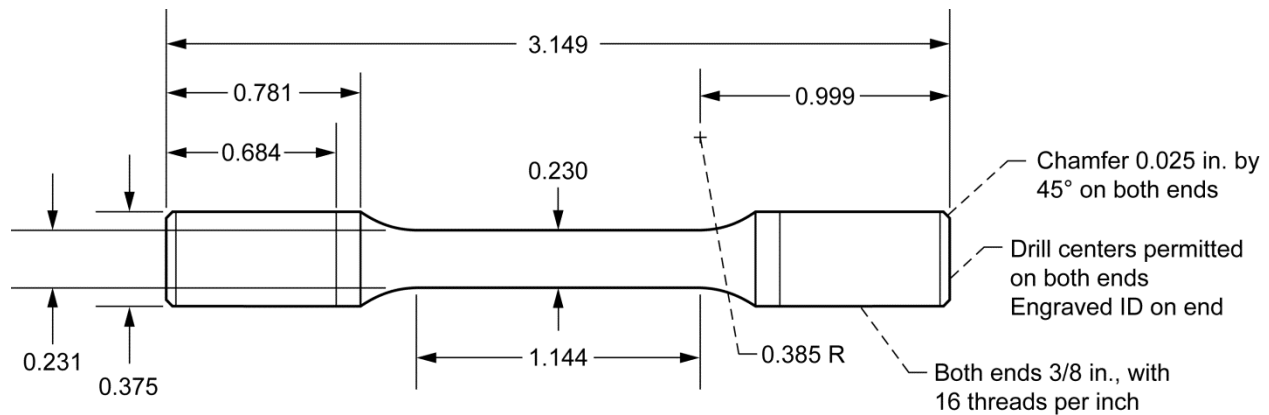
Figure 2.—Tensile and creep specimen design. All dimensions are in inches unless marked otherwise; scale is 1:1.

2.4 Tensile Testing

Tensile testing was conducted at room temperature and 500 °C (932 °F) using a modified Instron TT series load frame that allowed computer control and data acquisition using MTS Systems Corporation TestWorks 4 software. The software-frame combination also allowed strain rate control testing. A strain rate of 0.005 (mm/mm)/min was selected to be consistent with past GRCop-84 testing. For the room temperature testing, a clip-on MTS Model 634.12 extensometer was used to measure the strain.

For testing at 500 °C, an MTS 632.59B–04 high-temperature water-cooled extensometer was used. The sample was heated to temperature at a rate of at least 1000 °C/h (1800 °F/h), stabilized for 5 min, and tested. Ar was flowed through the furnace cavity at a rate between 1 and 2 liters/min (0.4 to 0.8 SCFM) to minimize oxidation, which would change the cross section of the samples.

The design shown in Figure 2 was used for both room and elevated temperature tensile testing. The design is consistent with ASTM E8 (Ref. 18). The design also was used in past GRCop-84 testing. Five sets of samples were made from as-extruded material and from material aged at 425 and 525 °C for 30 and 90 min.

2.5 Creep Testing

Vacuum creep testing was conducted to determine the steady-state creep rate and creep life. A temperature of 500 °C (932 °F) was selected to both provide a direct comparison to past GRCop-84 testing and to provide a temperature low enough to highlight the anticipated benefits of the Zr addition. Three stresses were selected: 109.2, 125.5, and 144.5 MPa (15.8, 18.2, and 20.9 ksi). These stress levels were again consistent with past GRCop-84 creep testing and would provide direct comparisons to the baseline alloy. Duplicate tests were conducted for as-extruded samples and samples aged at 425 and 525 °C for 30 and 90 min. The design shown in Figure 2 also was used for the creep specimens.

Vacuum creep testing was conducted in test frames from the Brew Corporation. The vacuum chamber was evacuated to a pressure below 1.3 mPa (1×10^{-5} torr), with most tests being conducted near 0.4 mPa (3×10^{-6} torr). The sample was heated to temperature at a rate of at least 1000 °C/h (1800 °F/h). The temperature of the sample was measured and controlled using a Type R (Pt/Pt-13 wt% Rh) thermocouple tied to the center of the sample.

During heating, a small load equivalent to 0.5 kg (1 lb) was applied to keep the load train aligned under a slight tension. Once at temperature, the sample temperature was stabilized, and the preload was removed. The weight pan was raised with a jack, the proper mass was placed on the pan, and the pan was lowered again with the jack. For consistency and quickness, an electric drill was used to raise and lower the weight pan at a constant rate. A 10:1 load arm was used, so a weight 1/10th of the desired sample load was used in the weight pan. A Honeywell Sensotec Type 31 precision miniature load cell in the load train allowed for monitoring and recording the actual applied load.

A linear variable resistor (LVR) was attached to the load frame outside of the chamber to measure the creep strain. Because it was outside of the chamber, the sensor measured the total displacement of the load train, which included any slack in the system and any deformation that occurred outside of the reduced section. The slack appeared as a large initial change in position. It is likely that most of the displacement recorded in the first one or two data points following application of the load came from the removal of this slack. The deformation outside of the reduced section was miniscule (Ref. 19) and was ignored in the calculation of the creep strain.

An Optical Gaging Products Focus Contour Projector optical comparator was used to determine the initial length of the reduced section. The creep strain was calculated by dividing the total displacement by the initial reduced section length. The steady-state creep rate was determined by calculating the slope of the creep curve (creep strain versus time) in the region where the curve was linear and exhibited a minimum in the slope of the curve. All samples exhibited a lengthy steady-state regime, so there was no difficultly in identifying the section of the curve to be used in calculating the steady-state creep rate.

Data were acquired with a custom data acquisition (DAQ) system and associated software. The DAQ system measured and recorded the sample temperature in three sample locations, as well as the vacuum, displacement, and load. Typically, data were recorded every second during the first 5 min and every 10 or 15 min thereafter. The DAQ system also interrogated the instruments every 10 s and stored the data in a ring buffer. Upon detecting failure, as defined by a 90-percent decrease in the load channel reading, the data for the past hour that had been stored in the ring buffer were also recorded to the data file. This allowed excellent resolution of the creep life and extra detail in the creep curve immediately prior to failure.

Equation (1) was entertained to determine if the Zr addition and the aging heat treatments had any effect on the creep properties:

$$\log_{10}(Y) = \beta_0 + \beta_1 \log_{10}(\sigma) + \beta_2 B_1 \log_{10}(\sigma) + \beta_3 B_2 \log_{10}(\sigma)$$
$$+ \beta_4 B_3 \log_{10}(\sigma) + \beta_5 B_4 \log_{10}(\sigma) + \beta_6 B_5 \log_{10}(\sigma) \tag{1}$$

Here Y is the response variable (creep rate in inverse seconds or creep life in hours), and σ is the applied stress in megapascals, β_0 to β_6 are the coefficients for the terms, and B_1 to B_5 are blocking variables representing the aging heat treatments shown in Table II. A blocking variable was set to 1 if the specimen had that heat treatment and to 0 if it did not. If all blocking variables were 0, then the sample was a GRCop-84 specimen in the as-extruded condition. The as-extruded GRCop-84 was used as the baseline for the comparison.

By using forward stepwise regression, it is possible to determine which terms are statistically significant and which are not. Terms with a blocking variable that enter the final regression model indicate that the condition corresponding to that blocking variable produced a statistically significant change in the response variable. The sign of the coefficient of the term β_x indicates if the change is beneficial or detrimental. By including the baseline as-extruded GRCop-84Z data and comparing it with the as-extruded GRCop-84 data, it is possible to determine if adding Zr alone produces a significant difference or if aging is required.

TABLE II.—GRCop-84Z HEAT TREATMENTS CORRESPONDING
TO EQUATION (1) BLOCKING VARIABLES

Blocking variable	Heat treatment
B_1	As received
B_2	425 °C/30 min/air cooled (AC)
B_3	425 °C/90 min/AC
B_4	525 °C/30 min/AC
B_5	525 °C/90 min/AC

2.6 Low Cycle Fatigue Testing

So that material would be conserved and tests would be consistent with past GRCop-84 LCF testing, specimen blanks approximately 1.2 cm in diameter by 6.4 cm long (0.46 in. in diameter by 2.5 in. long) were wire electrical discharge machined from the as-extruded and the heat-treated GRCop-84Z bars. Type 310 stainless steel extensions were inertia welded onto both ends by Interface Welding of Carson, California, to extend the length of the samples to approximately 15.2 cm (6 in.).

The samples were machined to the design shown in Figure 3. As with tensile and creep testing, samples were tested in the as-extruded condition and following aging at 425 and 525 °C for 30 and 90 min. Aging was done prior to inertial welding to prevent any distortion or other problems with thermal expansion mismatch between the GRCop-84Z and the Type 310 stainless steel that might be encountered in a post-machining heat treatment.

LCF testing was done at Glenn using a hydraulic MTS load frame. The specimens were tested in strain control with the strain being measured by an MTS 632.53 extensometer. Total strain ranges $\Delta\varepsilon_{total}$ of 0.8, 1.0, and 1.2 were used in the testing, and the strain rate was 0.002 m/m/s in all tests. The testing used a fully reversed ($R = -1$) triangular waveform for the strain with no dwell. All testing was conducted at room temperature.

Heat treatment appeared to have some effect on the LCF lives of GRCop-84. Equation (2) was entertained to determine if there were statistically significant differences in the LCF lives of GRCop-84Z with various heat treatments and the baseline as-extruded GRCop-84:

$$\log_{10}(\Delta\varepsilon_T) = \beta_0 + \beta_1 \log_{10}(\text{life}) + B_1\beta_2 + B_2\beta_3 + B_3\beta_4 + B_4\beta_5 + B_5\beta_6$$
$$+ B_1\beta_7 \log_{10}(\text{life}) + B_2\beta_8 \log_{10}(\text{life}) \tag{2}$$
$$+ B_3\beta_9 \log_{10}(\text{life}) + B_4\beta_{10} \log_{10}(\text{life}) + B_5\beta_{11} \log_{10}(\text{life})$$

Here $\log_{10}(\Delta\varepsilon_T)$ is the common logarithm of the strain range, $\log_{10}(\text{life})$ is the common logarithm of the life, B_1 to B_5 are blocking variables representing the various heat treatments of the GRCop-84Z specimens, and β_0 to β_{11} are the coefficients to be fit through the regression analysis. If the blocking variable was 1, the specimen received the heat treatment represented by the blocking variable as shown in Table II. If all the blocking variables were 0, the data point was for the baseline as-extruded GRCop-84.

A forward stepwise regression analysis was conducted using SigmaStat Version 3.5. For this analysis, F statistic values (the value of the F distribution for X degrees of freedom associated with the numerator and Y degrees of freedom associated with the denominator) of 4 to enter and 3.9 to leave were selected. These values correspond to an approximate 95-percent confidence that the variable should be included or excluded. The inclusion of terms with one of the blocking variables indicates that the corresponding aging heat treatments had a statistically significant effect upon the LCF properties.
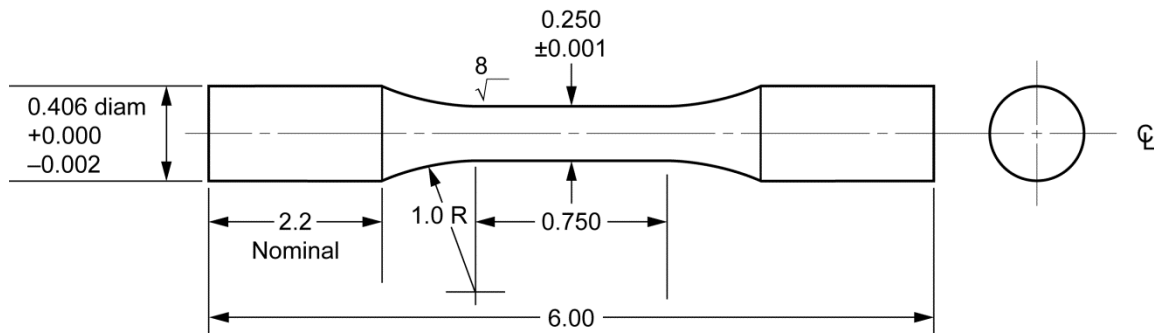
Figure 3.—Low cycle fatigue specimen design. All dimensions are in centimeters; ₵ indicates the centerline.

Equation (3) was modified to examine if the stress range for GRCop-84Z was statistically different from as-extruded GRCop-84:

$$\log_{10}(\Delta\sigma) = \beta_0 + \beta_1 \log_{10}(\Delta\varepsilon_P) + B_1\beta_2 + B_2\beta_3 + B_3\beta_4 + B_4\beta_5 + B_5\beta_6$$
$$+ B_1\beta_7 \log_{10}(\Delta\varepsilon_P) + B_2\beta_8 \log_{10}(\Delta\varepsilon_P) \qquad (3)$$
$$+ B_3\beta_9 \log_{10}(\Delta\varepsilon_P) + B_4\beta_{10} \log_{10}(\Delta\varepsilon_P) + B_5\beta_{11} \log_{10}(\Delta\varepsilon_P)$$

where $\log_{10}(\Delta\sigma)$ is the natural logarithm of the stress range, $\log_{10}(\Delta\varepsilon_P)$ is the natural logarithm of the strain range, and B_1 to B_5 are the blocking variables given in Table II. A forward stepwise regression analysis was conducted using SigmaStat and the F values to determine if there was a statistically significant difference between the as-extruded GRCop-84 and the GRCop-84Z with the various heat treatments.

2.7   Optical Microscopy

In addition to mechanical testing, optical microscopy was used to examine the alloy in the as-extruded and heat-treated conditions. Samples were mounted in Bakelite (Union Carbide and Carbon Corporation) or epoxy and were mechanically polished through 0.05-μm colloidal silica using the same procedures used with GRCop-84. The material was etched using a solution of 25-ml NH_4OH—50 ml $(NH_4)_2S_2O_8$ solution (2.5 g/100 ml solution)—25-ml H_2O that was diluted by adding 5 parts distilled water to 1 part etchant. Dilution was required to prevent overetching the samples. A Reichert ME3 metallograph was used for all optical observations.

2.8   X-Ray Mapping

The optical microscopy samples were also examined in a JEOL 840A Scanning Electron Microscope. X-ray mapping was used to assess the qualitative abundance of Cu, Cr, Nb, and Zr in the observed phases.

3.0   Results

The following subsections give results for the microstructural evaluation and the mechanical properties. No results are presented for cold-worked GRCop-84Z because the task was terminated before samples could be produced and tested.

3.1   Chemical Composition

Table III presents the chemical composition of the starting powder provided by ATI Powder Metals. The composition of the extruded bar, which was measured at Glenn, also is shown, and for reference, the target composition is presented. The results show that the composition of the GRCop-84Z produced is very close to the desired composition.

TABLE III.—GRCop-84Z CHEMICAL COMPOSITION

Composition, wt% (at.%)						
Element						
Cr	Nb	Fe	Hf	O	Zr	Cu
Target						
6.65 (8.17)	5.85 (4.02)	<0.0050	<0.0020	<0.0400	0.35 (0.25)	Balance
Crucible Research powder						
6.75 (8.29)	5.86 (4.03)	0.004	0.005	0.0205	0.44 (0.31)	Balance
Glenn extruded bar						
6.61 (8.12)	5.86 (4.03)	<0.005	<0.001	0.0103	0.43 (0.30)	Balance

The amount of Zr is slightly higher than the target of 0.35 wt% but well within the range of 0.25 to 0.5 wt% used to specify the alloy for production. In this case, a slight excess of Zr was deemed to be desirable since uniformly adding Zr to Cu alloys during production can be difficult. It is likely that practices can be developed to adjust the addition to the desired level with additional production heats.

The remaining elements fall well within the historical ranges for GRCop-84. Oxygen was low and remained so after consolidation. Fe from the Cr melt stock was present at a very low level as well. Other trace impurities associated with the refractories used for the melting were not present at detectable levels.

In addition to the normal impurities for GRCop-84, a small amount of Hf from the Zr melt stock was detected in the powder sample but not in the consolidated material. Lack of Hf in the extruded bar analysis is probably a detection limit issue rather than an actual lack of Hf because it is known that some Hf entered the alloy with the Zr and a small amount was detected in the powder sample. The difference was not considered to be significant.

3.2   Powder Sieve Analysis

The sieve analysis, presented in Table IV, shows that 57.2 percent of the powder was –325 mesh, or less than 44 μm in diameter. This is a greater proportion of –325 mesh powder than is typically observed for GRCop-84 atomized under similar conditions. However, the maximum size of the powder particles based on the sieve analysis was 125 μm, which is slightly greater than the desired 105-μm diameter specified. The fraction of the oversize powder was small (2.4 percent) and was not considered to be significant.

TABLE IV.—SIEVE ANALYSIS OF GRCop-84Z POWDER

Sieve size	----- +120	–120 +140	–140 +200	–200 +230	–230 +270	–270 +325	–325 -----
Nominal diameter range, μm	>125	105 to 125	74 to 105	62.5 to 74	53 to 62.5	44 to 53	<44
Percent of particles in range	0	2.4	16.2	9.8	6.7	6.2	57.2

Anecdotal evidence from the loading of the extrusion can and handling of the powder, such as a lower packing factor for GRCop-84Z (0.63 versus 0.67), also indicates that the GRCop-84Z powder was finer than similarly atomized GRCop-84 powder. It appears that the addition of Zr had the unintended effect of increasing the fluidity of the molten metal and improving the atomization of the powder.

3.3   Phases Present

Figure 4 shows the x-ray diffraction results from the as-extruded GRCop-84Z. The major phases present were Cu and Cr_2Nb. This is consistent with the results obtained for GRCop-84, the base of GRCop-84Z. The relative intensities of the two phases were very large compared with the minor phases identified.

The four minor phases identified were Cr, $CuZr_2$, Cu_5Zr, and $Nb_{0.6}Cr_{0.4}O_2$. Elemental Cr was present because there was a slight excess of Cr in the alloy to lower the activity of Nb in the Cr_2Nb and prevent possible hydrogen embrittlement. The $Nb_{0.6}Cr_{0.4}O_2$ was most likely a tenacious surface oxide that either was not completely removed from the sample or that formed during the course of the scans. It also may have been incorporated oxide from the powder that had 205 ppm O.

$CuZr_2$ was not expected because it is the most Zr-rich of the several Cu-Zr compounds. It may be indicative of Zr entering the melt and not being well dissolved and mixed prior to atomization. Subsequent solution heat treatments would probably dissolve the Zr into the Cu as a solid solution and reduce or eliminate this phase. Because of this, it is not considered to be a major strengthening phase for GRCop-84Z and will not be included in the discussion even though a small amount still may be present. Cu_5Zr has been observed in the past in Cu-Cr-Zr alloys (Ref. 9). From the Cu-Zr phase diagram (Ref. 6), the expected phase was Cu_9Zr_2 for a low-Zr alloy. It appears that the presence of Cr modifies the activities of Cu and Zr such that the formation of Cu_5Zr is favored over Cu_9Zr_2.

DE GRCop-842 SS10 3scan merge

■ Copper, syn (01-071-7905)   ■ Copper zirconium (04-002-0044) 9.7%
■ Chromium niobium (01-074-6798)   ■ Copper zirconium (04-004-4637) 89.9%
■ Chromium, syn (04-004-2040) 0.4%   ■ Niobium chromium oxide (00-031-0927)
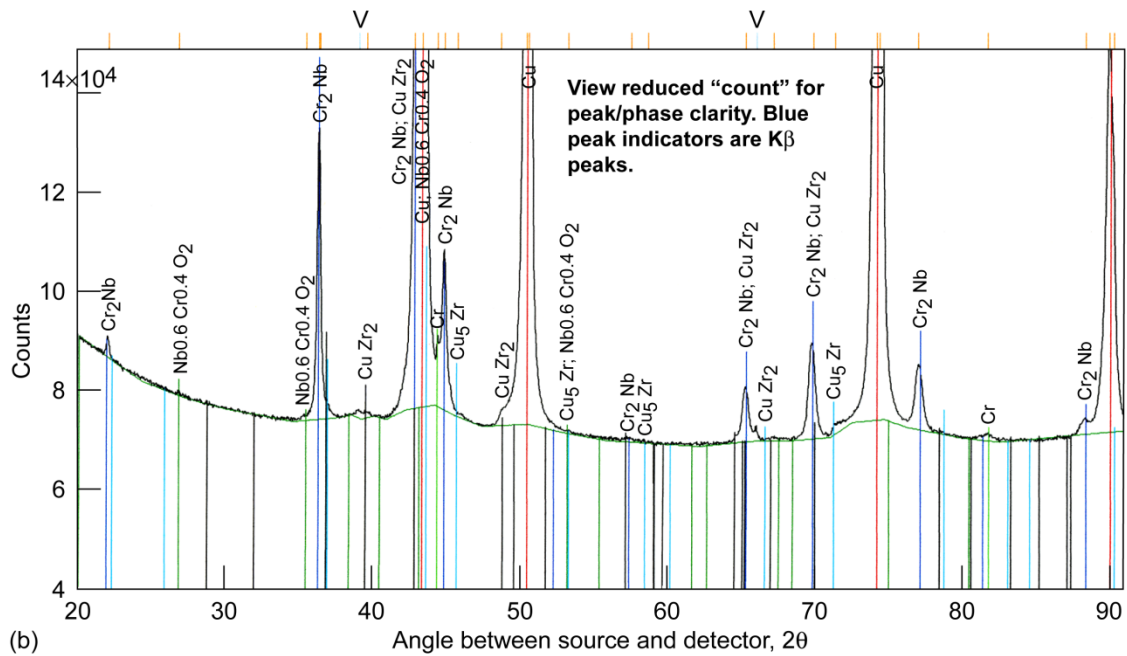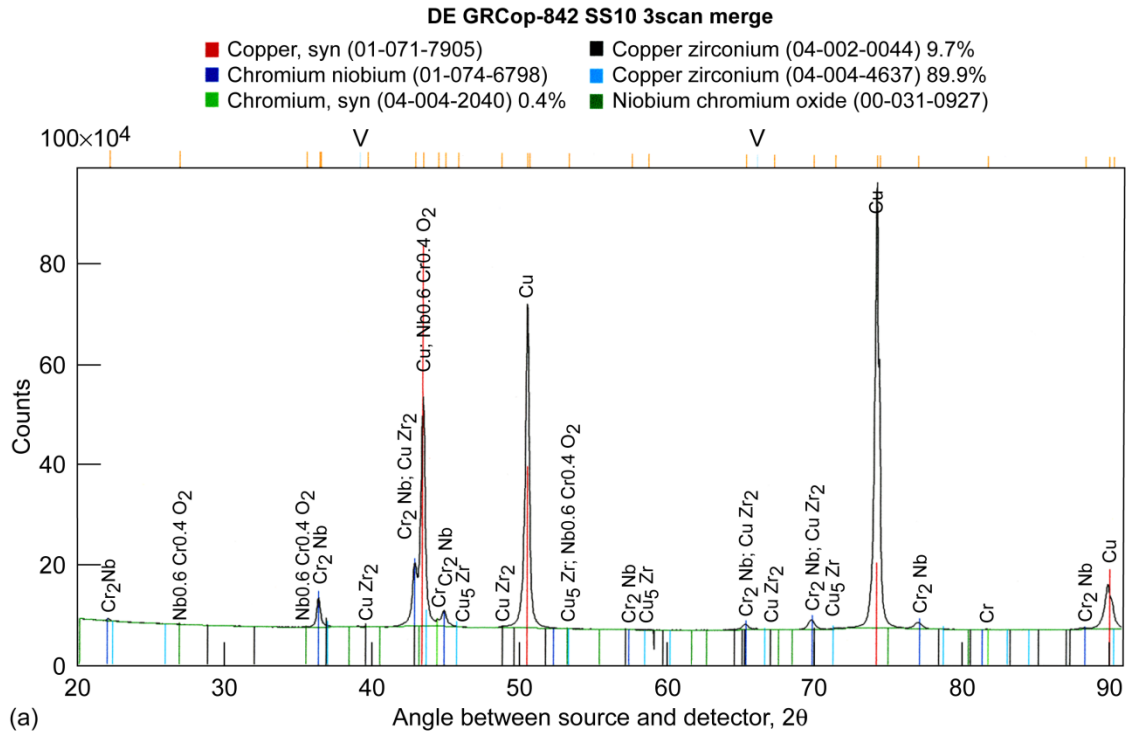
Figure 4.—X-ray diffraction scan results. (a) Overview of results. (b) Detail of results highlighting minor phase peaks.

3.4   Heat Treatment Development

The hardness data from the solution heat treatments (SHTs) were analyzed using an Analysis of Variance (ANOVA) test to determine if statistically significant differences at a 95-percent confidence level existed in the hardnesses measured before and after the heat treatments. Table V shows the average

hardness for the as-received and solution-heat-treated conditions and the results of the ANOVA. For an F value of 1.8, no statistically significant differences were observed between the conditions in the study, so optical microscopy and metallurgical principles were used to determine the solution heat treatment temperature.

TABLE V.—ANALYSIS OF VARIANCE (ANOVA) RESULTS
FOR SOLUTION-HEAT-TREATED GRCop-84Z

Group name[a]	Number of readings	Mean Rockwell B hardness, HR_B	Standard deviation of hardness, HR_B
As-received	10	68.99	3.41
900 °C SHT	9	67.45	3.20
925 °C SHT	10	69.46	2.39
950 °C SHT	10	70.38	1.29

[a]SHT, solution heat treatment.

Sources of variation	Degrees of freedom, ν	Sum of squares (SS)	Mean square (MS)	F value[b]	Probability
Between groups	3	39.465	13.155	1.843	0.158
Residual	34	242.629	7.136	--------	--------
Total	37	282.094	--------	--------	--------

[b]Value of the F distribution for X degrees of freedom associated with the numerator and Y degrees of freedom associated with the denominator.

Figure 5 shows typical optical micrographs from the as-extruded and solution-heat-treated samples. The microstructures exhibit a Cu matrix and readily discernable bluish-silver Cr_2Nb precipitates. In addition, there are smaller, dark-gray precipitates. X-ray maps of the as-extruded sample indicated that the small precipitates were rich in Zr. There was no indication of Zr in the other phases. This, along with the x-ray diffraction analysis, led to the identification of the smallest precipitates as Cu_5Zr. Examination of the micrographs indicates that there is apparently some decrease in the area fraction of Cu_5Zr precipitates as the solution heat treatment temperature increases. At 972 °C (1782 °F), the eutectic temperature, the solid solubility limit of Zr in solid Cu is 0.17 wt% (Ref. 6), so it is likely that there will always be some Cu_5Zr precipitates in the GRCop-84Z that cannot be dissolved. The solid solubility decreases rapidly at lower temperatures, so it was expected that more Cu_5Zr precipitates would be observed at lower solution heat treatment temperatures. This appears to be consistent with the observed microstructures.

The phase diagram, the composition of the alloy, and the optical microscopy were considered in the decision to use a solutioning temperature of 950 °C to maximize the amount of Zr that could be placed in solution. This was also considered to be a reasonable upper temperature limit to prevent incipient melting due to small fluctuations and spatial variances in the furnace temperature.

With the solutioning heat treatment fixed at 950 °C/30 min/WQ, the aging heat treatment was examined. The hardness of the samples after solutioning and after aging were examined to determine if the hardness increased from the aging heat treatment. Because the variance of the hardness data was fairly high, a t-test between the data for the same sample in the solutioned condition and in the aged condition was used to determine if the measured differences were statistically significant. All data sets passed normality and equal variance testing. Table VI shows the results. In all cases the averages are statistically different, with the aged material being harder. In some cases the power of the test was lower than the desired value of 0.8, so there is a chance that there is a false positive in the results. Given that the trend is consistent and the expected result, this is not considered to be likely.

TABLE VI.—RESULTS FOR GRCop-84Z AGING HEAT TREATMENTS

Heat treatment[a]	Condition	Average Rockwell B hardness, HR_B	Standard deviation of hardness, HR_B	Increase in hardness, HR_B
425 °C/30 min/AC	SHT[b]	69.4	3.2	6.4
	Aged[c]	75.8	2.3	
425 °C/90 min/AC	SHT[b]	72.1	4.4	6.3
	Aged[c]	78.4	2.3	
475 °C/30 min/AC	SHT[b]	73.1	1.3	3.4
	Aged[c]	76.5	2.6	
475 °C/90 min/AC	SHT[b]	72.2	1.4	6.8
	Aged[c]	79.0	2.58	
525 °C/30 min/AC	SHT[b]	73.4	2.3	5.0
	Aged[c]	78.4	3.1	
525 °C/60 min/AC	SHT[b]	72.3	3.5	5.1
	Aged[c]	77.4	3.3	

[a]AC, air cooled.
[b]Solution heat treatment at 950 °C for 30 min, then water quenched.
[c]Aged using indicated heat treatment.
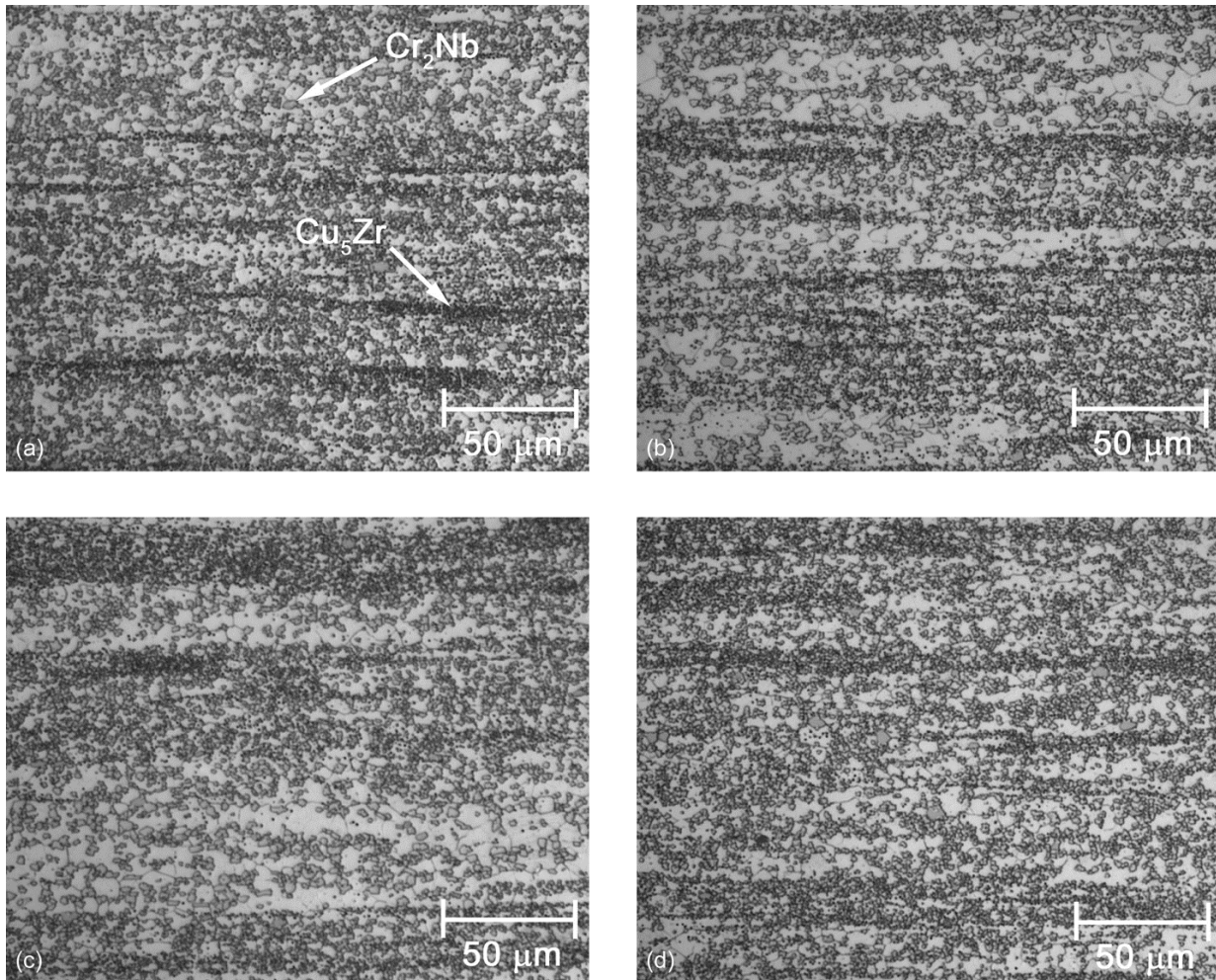
Figure 5.—Optical micrographs of solution-heat-treated GRCop-84Z samples. (a) As-extruded. (b) 900 °C/30 min/water quenched (WQ). (c) 925 °C/30 min/WQ. (d) 950 °C/30 min/WQ.

The hardness values show no clearly preferable aging temperature. They also show that the precipitation process is probably fast since the hardnesses at 30 min are nearly identical to those at 60 and 90 min. The growth kinetics do not appear to be fast because the longer times did not result in a large decrease in hardness due to substantial overaging.

Because of these results, material aged at 425 and 525 °C was selected for testing. The aging time was set to both 30 and 90 min to see if there were any discernable differences in tensile strength that would indicate a preferred time. The resulting mechanical property test matrix, therefore, had five heat treatment conditions: as-extruded, SHT/425 °C/30 min/AC, SHT/425 °C/90 min/AC, SHT/525 °C/ 30 min/AC, and SHT/525 °C/90 min/AC.

3.5   Tensile Testing

Figure 6 presents the results of the tensile testing as well as baseline GRCop-84 data as a comparison (Ref. 20). Figure 7 shows the relative change in the tensile properties.

At room temperature, the Zr-modified GRCop-84 exhibited less necking and failure at higher loads than did the baseline GRCop-84. The result was less reduction in area but more uniform tensile elongation. Although lower than desired, the reductions in area still ranged from 25 to 33 percent, so GRCop-84Z retained good, if somewhat lower, ductility. The deformation appeared to remain uniform with no instability for a longer time, and the tensile elongations increased as a result. Most tests were in the 25- to 28-percent range.
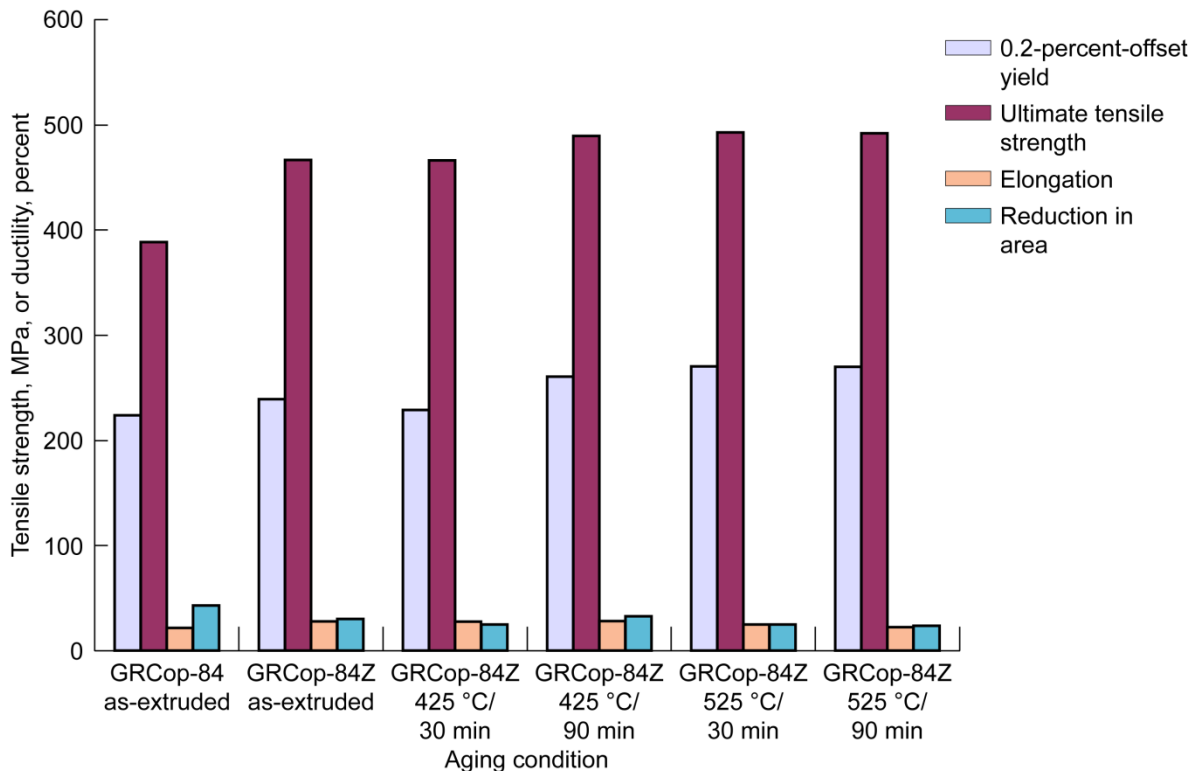
Figure 6.—Room temperature GRCop-84Z tensile test results.
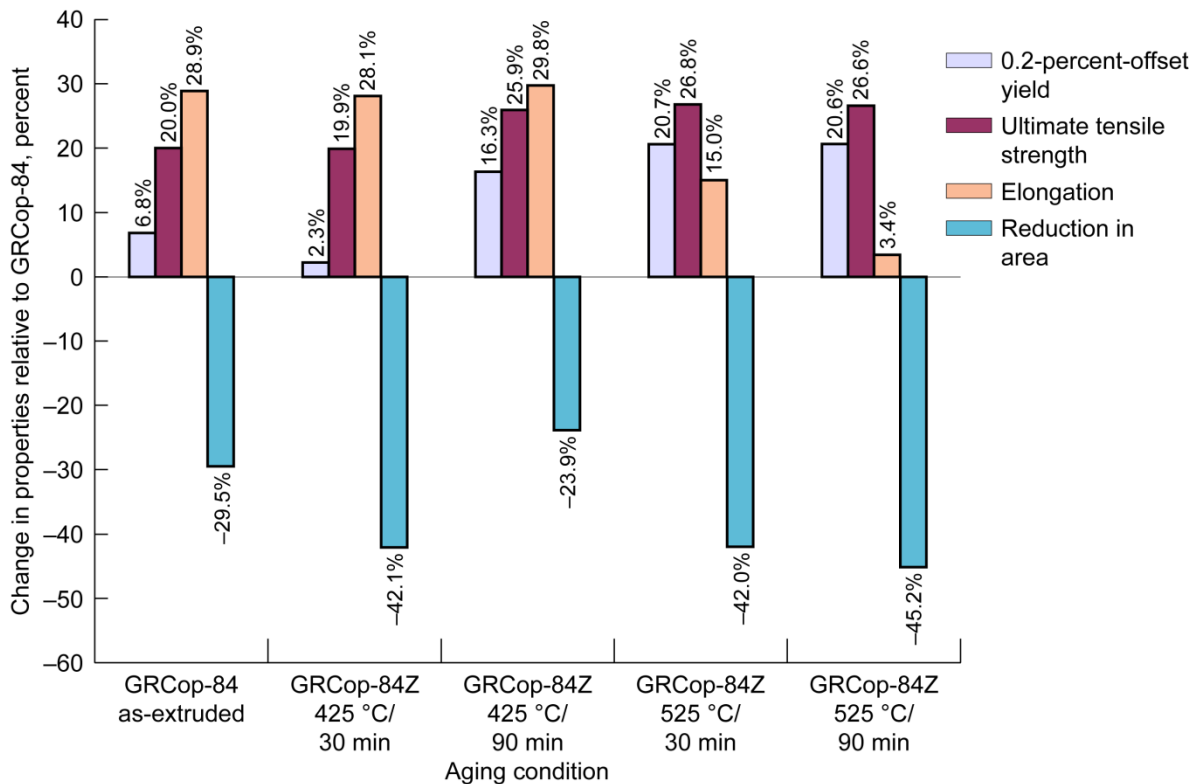
Figure 7.—Relative room temperature tensile properties of GRCop-84Z compared with baseline GRCop-84.

The room temperature 0.2% offset yield strength shows an increase for GRCop-84Z over GRCop-84 in all conditions. The 425 °C/30 min/AC condition has the least increase, which is consistent with the hardness data (Table VI) and is, in fact, lower than the as-extruded GRCop-84Z. This might indicate a failure to precipitate the Cu_5Zr phase completely after the solution heat treatment or insufficient growth of the precipitates to a size that provides the best impediment to dislocation motion. The 425 °C/90 min/AC heat treatment achieved the goal of a 15-percent increase in the room temperature yield strength. Both 525 °C aging heat treatments produced an increase in yield strength of 20 percent, so they meet the yield strength goal as well.

The strongest room temperature strength benefit of adding Zr was seen in the ultimate tensile strength (UTS). For all conditions tested, the UTS increased by 20 to 29 percent in comparison to the baseline GRCop-84. There was no goal for increasing the UTS, but this is a benefit for the material in many potential applications, such as those discussed in the Introduction.

At 500 °C, the Cu_xZr precipitates were anticipated to coarsen and produce less strengthening. However, Figure 8 shows a strong, positive effect of the Zr addition on all tensile properties. Figure 9 shows the change in properties relative to the baseline GRCop-84 properties.

Ductility was increased greatly relative to GRCop-84. At 500 °C the elongation increased by over 50 percent, and the reduction in area generally doubled.

The 500 °C 0.2% offset yield strength showed an increase of 25 percent for the as-extruded material and an increase between 37 and 64 percent for the aged material relative to GRCop-84. These results indicate that in the short term the Cu_xZr precipitates do not coarsen to the point that overaging occurs. This is consistent with the hardness measurements, which indicated slow growth kinetics.

The 500 °C UTS data indicate that the addition of Zr has a pronounced positive effect. In the as-extruded condition, the UTS increased by 24 percent in comparison to GRCop-84. Much more dramatically, the UTS increased between 43 and 68 percent for the aged GRCop-84Z specimens.
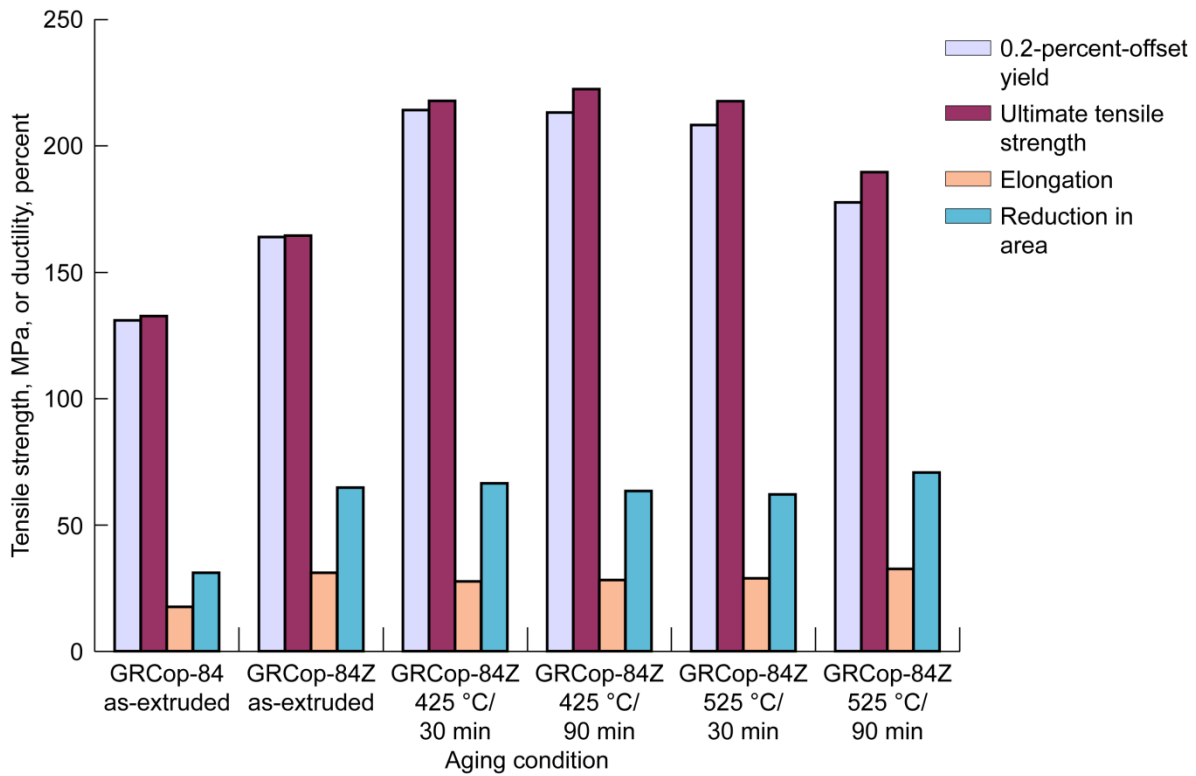
Figure 8.—500 °C GRCop-84Z tensile test results.
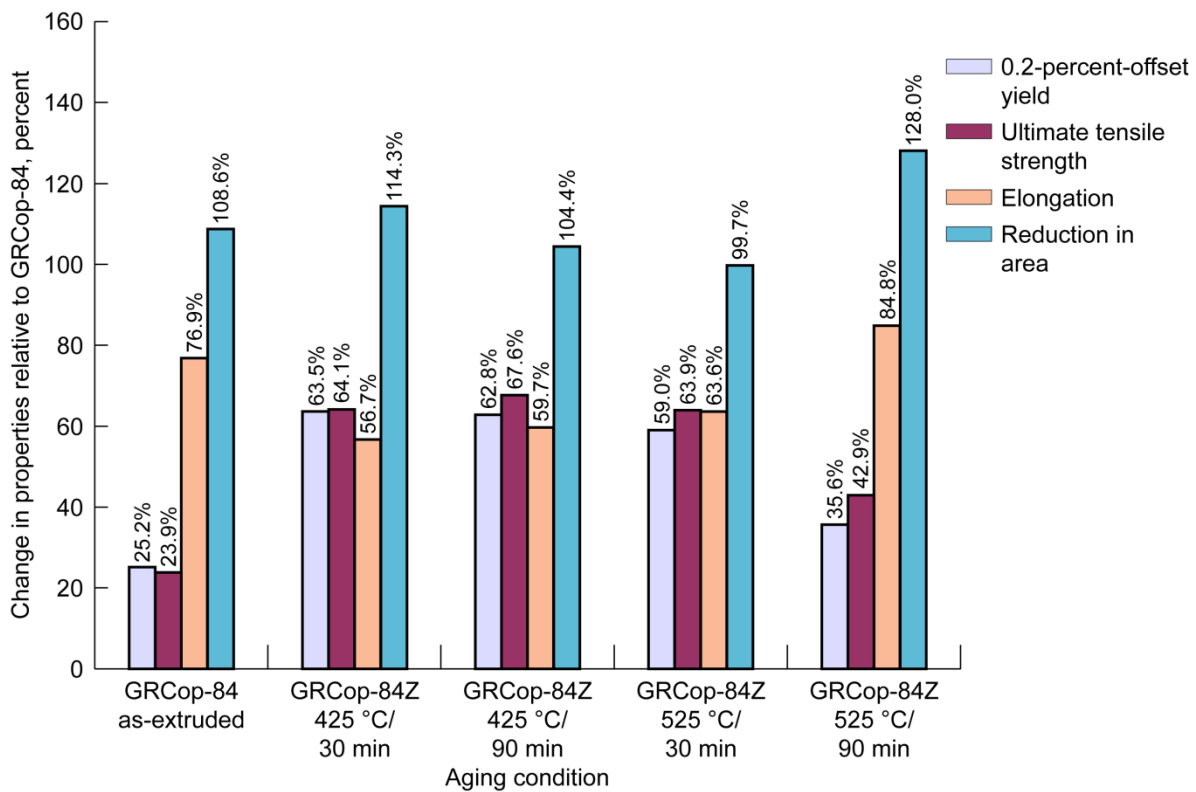
Figure 9.—Relative 500 °C tensile properties of GRCop-84Z compared with those of baseline GRCop-84.
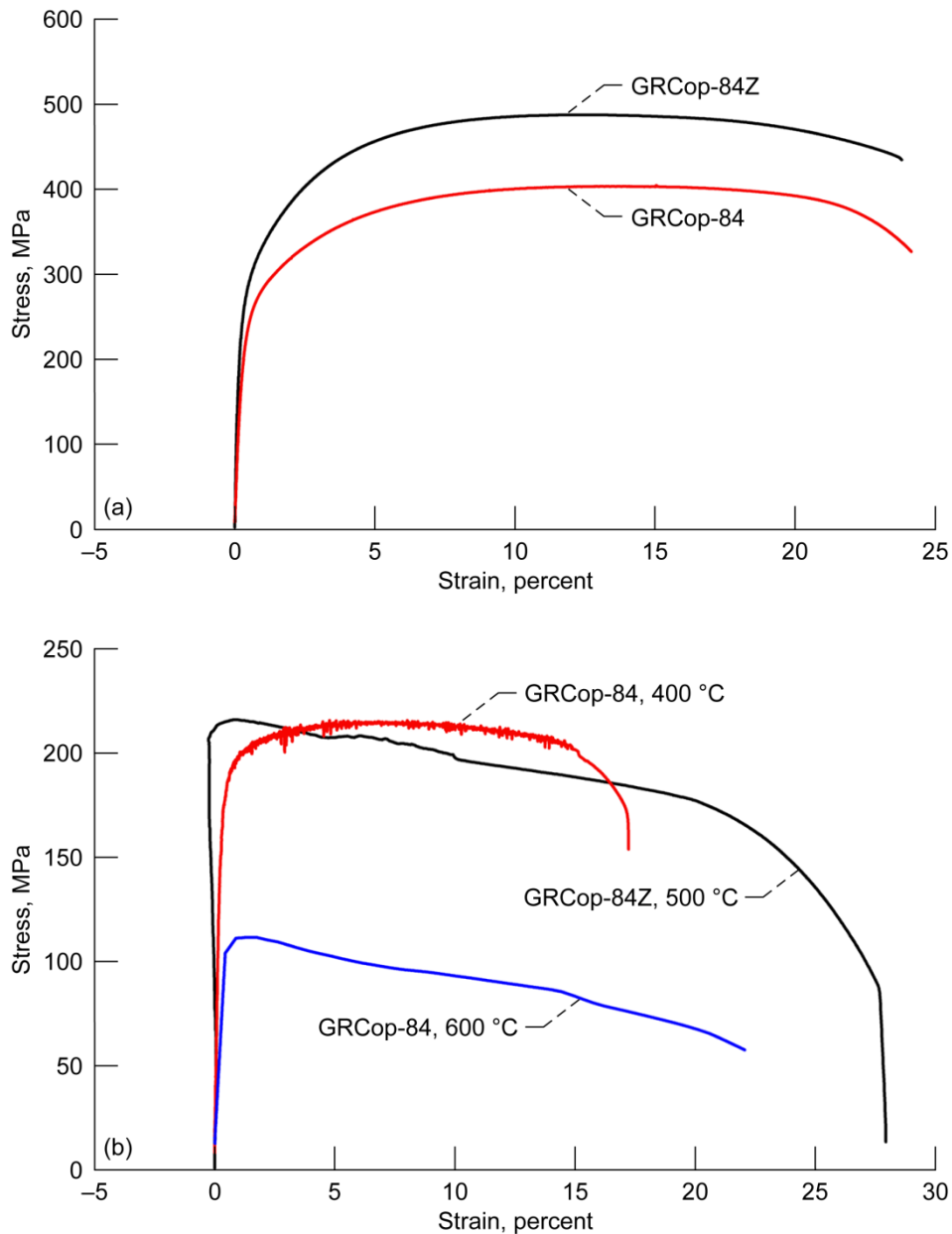
Figure 10.—Typical GRCop-84Z stress-strain curve. (a) Curve at room temperature
for sample Z–T4–525–90–2 with solution heat treatment of 950 °C/30 min/water
quenched and age of 525 °C/90 min/air cooled (AC). (b) Curves at 500 °C for sample
Z–T2–425–30–2 with solution heat treatment of 950 °C/30 min/water quenched
and age of 425 °C/30 min/AC.

Figure 10 shows typical room temperature and 500 °C stress-strain curves. For comparison, typical
GRCop-84 stress-strain curves are also presented in the plots. The room temperature stress-strain
behavior of GRCop-84Z is typical for most ductile materials and is consistent with GRCop-84. The
500 °C tensile curve is markedly different and atypical. The specimens undergo a near linear increase
until the yield strength is exceeded, and a relatively small strain between yield and ultimate tensile loads
occurs. The sample continues to elongate after the UTS is exceeded, and necking begins. The deformation

is considerable and accounts for most of the observed ductility. This is not consistent with typical 400 °C GRCop-84 stress-strain curves, though it is similar to the 600 °C stress-strain curves. The cause for this change in shape is not understood at the present time.

3.6   Creep Testing

Figure 11 shows a typical GRCop-84Z creep curve. The GRCop-84Z creep curves were very similar in shape to the GRCop-84 creep curves. Both normally exhibited a primary creep regime lasting about 10 percent of the total life followed by steady-state and tertiary creep regimes that were nearly equal in duration. Transitions between the regimes were gradual. As a result, the steady-state creep rate was taken from only the portion of the curve that had plainly achieved linearity.

Figure 12 shows the creep rate plotted against the creep life for GRCop-84Z samples in the as-extruded and aged conditions. The results for as-extruded GRCop-84 are also presented for comparison. The data were first examined as three data sets (as-extruded GRCop-84, as-extruded GRCop-84Z, and aged GRCop-84Z). The Monkman-Grant (Ref. 21) regression lines for the three data sets were coincident, so it was determined that the three data sets could be pooled.

The regression line for the pooled data with a 95-percent confidence interval is presented in Figure 12. The regression equation has a life exponent of −1.17±0.10 compared with −1.11±0.04 for GRCop-84 (Ref. 22). Although there was no statistically significant difference in the two slopes, the small dissimilarity was investigated further to see if it was possible to explain the difference. Examination of the plot in Figure 12 shows one data point that lies on the lower 95-percent confidence limit line. This data point was not treated as an outlier and was included in all subsequent analyses because there was no clear experimental or other reason to exclude the test results. The data point does influence the slope, and its removal does increase the slope to −1.16, but it alone does not explain the small change in slope. Without additional testing, it is not possible to determine if there is an effect on the Monkman-Grant curve from the Zr. Regardless, the change in slope does not represent a major difference from an engineering standpoint.
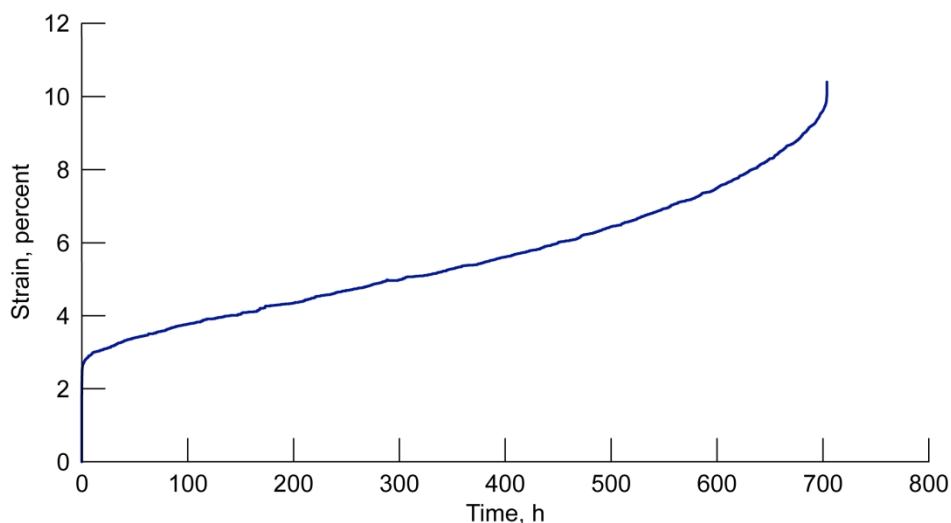
Figure 11.—Typical GRCop-84Z creep curve for GRCop-84Z specimen aged at 425 °C/30 min/air cooled and tested at 500 °C/125.6 MPa.
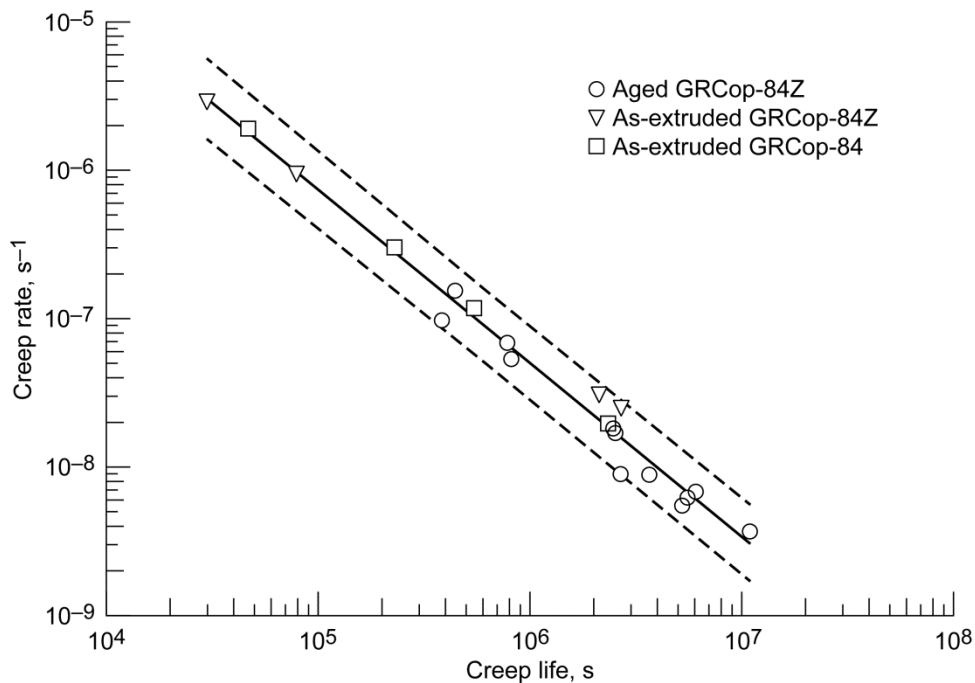
Figure 12.—GRCop-84Z Monkman-Grant curve. Creep rate = $10^{-0.286}$(creep life$^{-1.17}$); coefficient of determination, $R^2 = 0.9832$.

The data presented in Figure 13 clearly demonstrate that the aged GRCop-84Z creep properties are much improved over the GRCop-84 creep properties. The as-extruded GRCop-84Z test results were more complex. The as-extruded GRCop-84Z specimens tested at 125 and 144 MPa were comparable in life to the baseline as-extruded GRCop-84 data. However, the as-extruded GRCop-84Z specimens tested at 109 MPa demonstrated rates and lives more consistent with the aged GRCop-84Z. It appears that there was a change in the creep mechanism or dislocation movement between 109 and 125 MPa for GRCop-84Z at 500 °C. This observation needs to be further explored to better understand how the Zr affects and benefits the creep properties.

The similarities for the aged GRCop-84Z results led to the decision to examine just the aged specimen data to see if the four data sets were statistically different. A forward stepwise regression analysis was conducted using a simplified version of Equation (1) with three blocking variables and just the four aged GRCop-84Z data sets. The results show that there were no statistically significant differences between the four aging treatments, so the aged GRCop-84Z data were pooled into a single data set.

The possible change in creep behavior of the as-extruded GRCop-84Z and the pooling of the aged GRCop-84Z data meant that the model in Equation (1) needed to be modified. Blocking variables B_2 to B_5 were reduced to just B_3, and B_3 was set to 1 if the GRCop-84Z had been aged and was set to 0 otherwise. The as-extruded GRCop-84Z data were subdivided into low (109-MPa) and high (125- and 144-MPa) stress regimes, and the model was adjusted to add new blocking variables B_1 (low-stress test) and B_2 (high-stress test) to account for the two creep regimes.
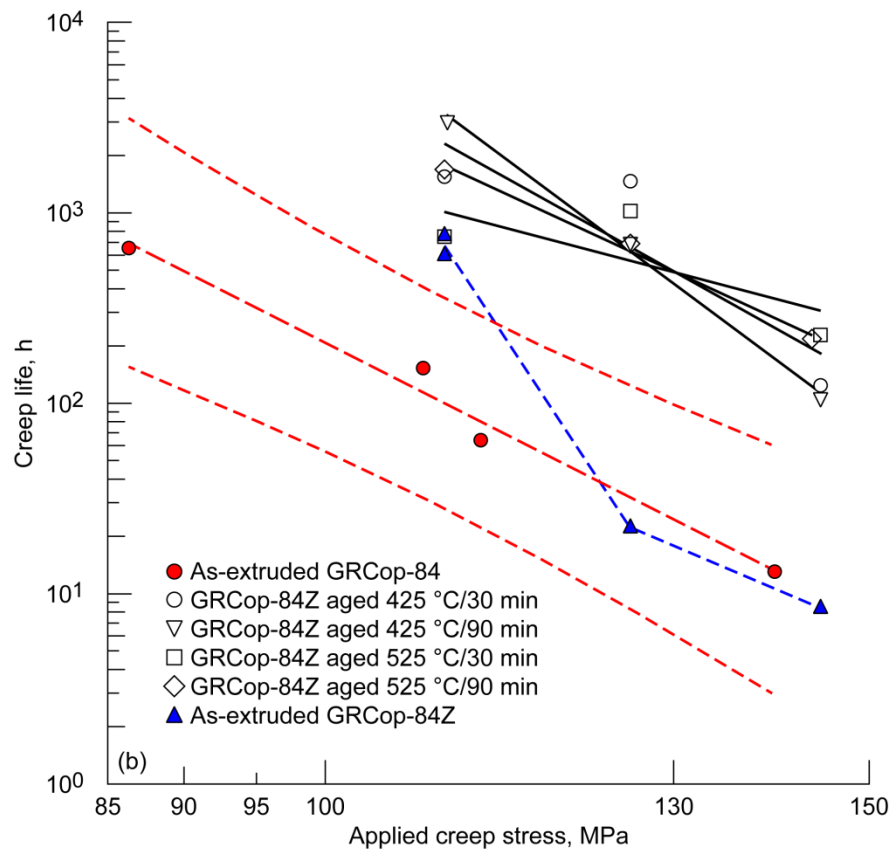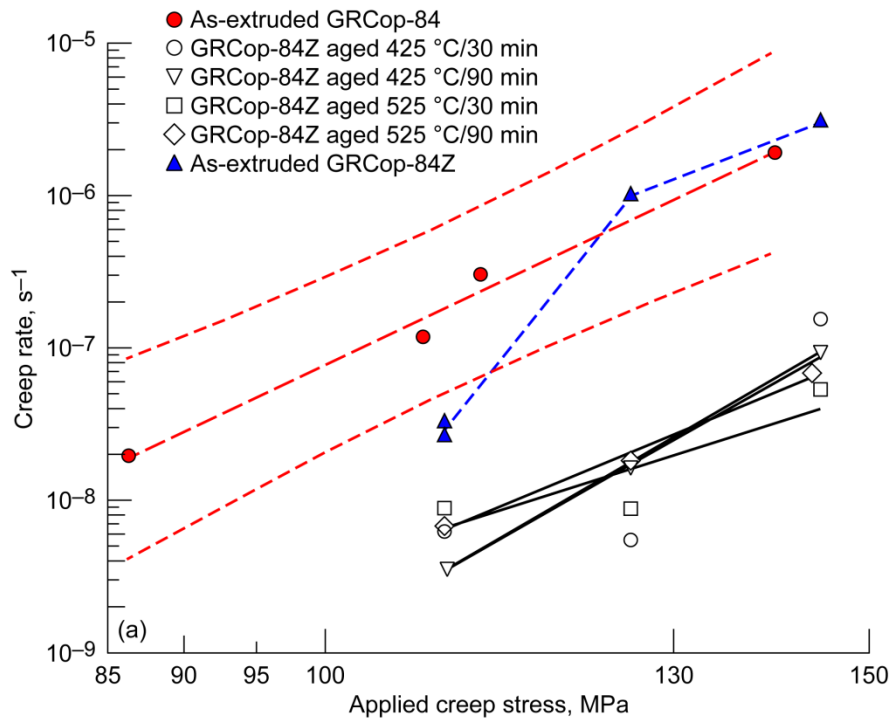
Figure 13.—Creep data for GRCop-84Z tested at 500 °C. (a) Creep rates. (b) Creep lives.

Table VII presents the results of the forward stepwise regression of the revised data sets. There are statistically significant differences between the low-stress, as-extruded GRCop-84Z and GRCop-84 and between the aged GRCop-84Z and the baseline GRCop-84Z. There is no statistical difference between the high-stress as-received GRCop-84Z and GRCop-84. This appears to be consistent with the data in Figure 13.

TABLE VII.—RESULTS OF FORWARD STEPWISE REGRESSION ANALYSIS OF CREEP DATA

(a) Creep rate.

[Coefficient of determination, $R^2 = 0.880$; standard error of estimate, $S_{Y.X} = 0.314$.]

Group[a]	Coefficient	Standard error	F value[b]	Probability
Constant	−27.230	1.722	-----------	---------
$\log_{10}(\sigma)$	10.060	.831	146.388	<0.001
$B_1\log_{10}(\sigma)$ (low-stress as-extruded)	−.401	.0843	22.641	<.001
$B_3\log_{10}(\sigma)$ (aged GRCop-84Z)	−.777	.0512	230.573	<.001

(b) Creep life.

[Coefficient of determination, $R^2 = 0.838$; standard error of estimate, $S_{Y.X} = 0.310$.]

Group[a]	Coefficient	Standard error	F value[b]	Probability
Constant	19.665	1.571	-----------	---------
$\log_{10}(\sigma)$	−8.678	.758	130.909	<0.001
$B_1\log_{10}(\sigma)$ (low-stress as-extruded)	.416	.0769	29.305	<.001
$B_3\log_{10}(\sigma)$ (aged GRCop-84Z)	.637	.0467	186.236	<.001

[a]σ, stress; B_1 and B_3, blocking variables indicating as-received material and material with a 425 °C/90 min/air cooled treatment, respectively.

[b]Value of the F distribution for X degrees of freedom associated with the numerator and Y degrees of freedom associated with the denominator.

Table VII also presents the standard error of estimate $S_{Y.X}$ and the coefficient of determination R^2 for the rate and life models. Both indicate a reasonably good fit of the revised data sets by the models. The remaining error for the models is about 1/3 order of magnitude, which represents the combined experimental error for the test rig and the random variability of the materials. The error term was consistent with prior GRCop-84 testing (Ref. 19) using the same test machines and probably represents the minimum achievable.

3.7   Room Temperature Low Cycle Fatigue Testing

Table VIII summarizes the LCF results, and Figure 14 presents the life as a function of total strain range. Prior as-extruded GRCop-84 room temperature LCF test data (Ref. 23) is presented as a baseline for comparison. The total strain range in this data set ranges from 0.004 to 0.06. The life scale was limited to better display the GRCop-84Z data, but all GRCop-84 data were used in the statistical analyses. The upper and lower 95-percent confidence limits for the as-extruded GRCop-84 data are also presented.

TABLE VIII.—LOW CYCLE FATIGUE TEST RESULTS SUMMARY
[Test temperature, 20 °C.]

Sample	Total strain,ᵃ Δεt, in./in.	Life, Nf, cycles	Rayleigh-Taylor modulus, Msi	First cycle, N = 1							Cycle at half life, Nf/2							Failure location
				Modulus, Msi	Strain range, Δεp, in./in.	Δεp/2, in./in.	Stress range, Δσ, psi	Δσ/2, psi	σmin, psi	σmax, psi	Modulus, Msi	Δεp, in./in.	Δεp/2, in./in.	Δσ, psi	Δσ/2, psi	σmin, psi	σmax, psi	
								As extruded										
T1–13	0.0070	16 502	17.24	17.00	0.0030	0.0015	64 591	32 296	–30 629	33 962	17.38	0.0028	0.0014	72 503	36 252	–36 087	36 416	Above top probe
T1–11	.0080	5 588	18.55	18.76	.0039	.0019	75 165	37 583	–36 501	38 664	18.72	.0036	.0018	80 978	40 489	–40 509	40 469	Above top probe
T1–12	.0100	5 586	19.22	18.89	.0056	.0028	78 011	39 006	–38 929	39 082	17.77	.0047	.0024	83 755	41 878	–41 955	41 800	Midgauge
T1–10	.0120	3 275	15.91	16.24	.0068	.0034	78 689	39 345	–38 556	40 133	16.40	.0066	.0033	87 308	43 654	–43 638	43 670	Midgauge
								Heat treatment, 425 °C/30 min										
T2–11	0.0080	7 622	18.45	18.07	0.0039	0.0020	69 732	34 866	–33 055	36 677	18.49	0.0036	0.0018	80 224	40 112	–39 939	40 285	At top probe
T2–12	.0100	2 595	19.48	19.09	.0057	.0029	76 706	38 353	–37 852	38 854	19.49	.0052	.0026	89 812	44 906	–44 993	44 819	Below bottom probe
T2–13	.0119	2 141	19.32	19.10	.0072	.0036	77 867	38 934	–38 042	39 825	17.75	.0067	.0034	91 065	45 533	–45 357	45 708	Above top probe
								Heat treatment, 525 °C/30 min										
T3–13	0.0080	7 714	18.78	19.33	0.0037	0.0019	77 175	38 588	–36 844	40 331	18.94	0.0034	0.0017	86 036	43 018	–42 998	43 038	Below bottom probe
T3–12	.0100	3 338	19.37	18.84	.0052	.0026	82 170	41 085	–40 135	42 035	18.24	.0048	.0024	93 667	46 834	–46 799	46 868	In gauge
T3–11	.0120	2 635	18.54	17.98	.0068	.0034	84 691	42 346	–41 903	42 788	17.89	.0065	.0032	97 501	48 751	–48 684	48 817	In gauge
								Heat treatment, 525 °C/90 min										
T4–10	0.0070	17 889	18.63	18.45	0.0026	0.0013	78 110	39 055	–38 037	40 073	18.41	0.0024	0.0012	84 580	42 290	–42 296	42 284	Above top probe
T4–12	.0080	9 352	18.54	18.61	.0034	.0017	79 092	39 546	–38 014	41 078	18.03	.0031	.0016	86 382	43 191	–43 562	42 820	Below bottom probe
T4–13	.0100	3 506	19.17	18.61	.0051	.0025	85 282	42 641	–41 584	43 698	18.13	.0047	.0023	95 259	47 630	–47 638	47 621	Above top probe
T4–11	.0120	1 853	19.47	19.38	.0068	.0034	91 168	45 584	–45 312	45 856	18.55	.0064	.0032	101 662	50 831	–50 817	50 845	Above top probe
								Heat treatment, 425 °C/90 min										
T5–12	0.0070	10 652	19.05	18.68	0.0027	0.0014	75 225	37 613	–35 189	40 036	18.52	0.0025	0.0012	83 096	41 548	–41 458	41 638	Midgauge
T5–10	.0080	5 538	18.83	18.61	.0033	.0017	81 744	40 872	–39 597	42 147	18.42	.0030	.0015	91 407	45 704	–45 695	45 712	Below bottom probe
T5–13	.0100	3 490	19.17	18.93	.0051	.0026	83 860	41 930	–40 919	42 941	18.19	.0048	.0024	93 931	46 966	–46 961	46 970	Above top probe
T5–11	.0120	1 496	19.95	19.40	.0067	.0034	90 555	45 278	–45 038	45 517	18.35	.0062	.0031	104 075	52 038	–51 940	52 135	Near top probe

ᵃTotal of the absolute values of the positive and negative strains.
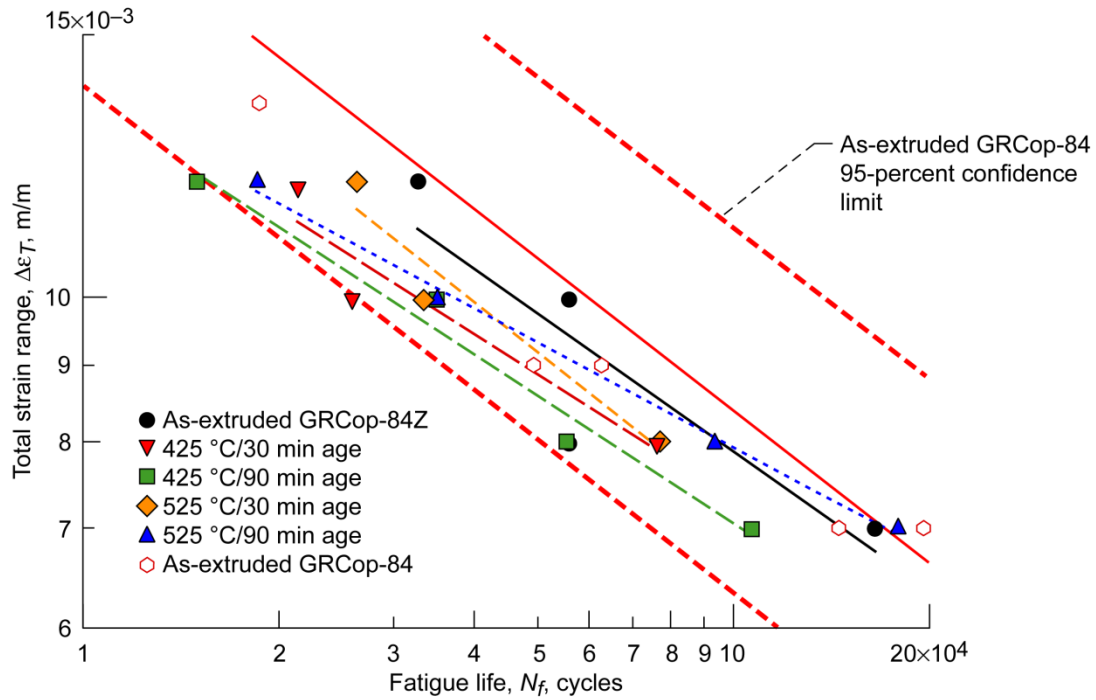
Figure 14.—Fatigue life as a function of total strain range.

Table IX gives the results for the forward stepwise regression analysis of the data fitted to the model in Equation (2). The negative coefficients indicate that, for a given life, the aging heat treatment lowered the strain range that could be sustained, or conversely, at a given strain range, the GRCop-84Z life was lower after receiving a 425 °C age. The exclusion of terms corresponding to the as-received and 525 °C aged GRCop-84Z samples indicates that, at a 95-percent confidence level, there were no statistically significant differences between GRCop-84Z in these heat-treated conditions and the baseline as-extruded GRCop-84.

Furthermore, no $B_x \log_{10}$(life) (where x = 1 to 5) terms made it into the regression model. These terms would indicate a change in slope for the regression lines corresponding to each condition. Since these terms do not enter the equation, there is a constant offset between the curves when there is a statistically significant difference in properties but no difference in the slopes. This indicates that there is no change in mechanism over the range of conditions studied.

Figure 15 shows the life as a function of plastic strain range at the half-life of the specimens. The two-sided 95-percent confidence limits for the as-extruded GRCop-84 data are also presented. The data show a similar result compared with the life as a function of the total strain (Figure 14). This was expected because, even at room temperature, both GRCop-84 and GRCop-84Z undergo little elastic deformation during LCF testing.

TABLE IX.—RESULTS OF FORWARD STEPWISE REGRESSION ANALYSIS
FOR LIFE VERSUS TOTAL STRAIN RANGE, $\Delta\varepsilon_T$

(a) Goodness of fit.

Multiple correlation coefficient, R	0.983
Coefficient of determination, R^2	.967
Adjusted R^2	.964
Standard error of estimate, $S_{Y.X}$	.0534

(b) Analysis of variance.

Group	Degrees of freedom	Sum of squares	Mean square	F value[a]	Probability
Regression	3	3.047	1.016	356.665	<0.001
Residual	37	0.105	0.00285	----------	---------

(c) Variables in model.

Variable[b]	Coefficient	Standard error	F value[a]	Probability
Constant	−0.727	0.0376	----------	---------
$\log_{10}$(life)	−.341	.0106	1036.543	<0.001
B_2	−.0721	.0322	5.021	.031
B_3	−.0806	.0283	8.119	.007

(d) Variables not in model.

Variable[b]	F value[a]	Probability
B_1	0.497	0.485
B_4	2.710	.108
B_5	1.930	.173
$B_1 \log_{10}$(life)	.464	.500
$B_2 \log_{10}$(life)	.253	.618
$B_3 \log_{10}$(life)	.449	.507
$B_4 \log_{10}$(life)	2.705	.108
$B_5 \log_{10}$(life)	1.468	.233

[a]Value of the F distribution for X degrees of freedom
associated with the numerator and Y degrees of freedom
associated with the denominator.
[b]B_1 to B_5 are blocking variables indicating the treatments
the material received (see Table II).
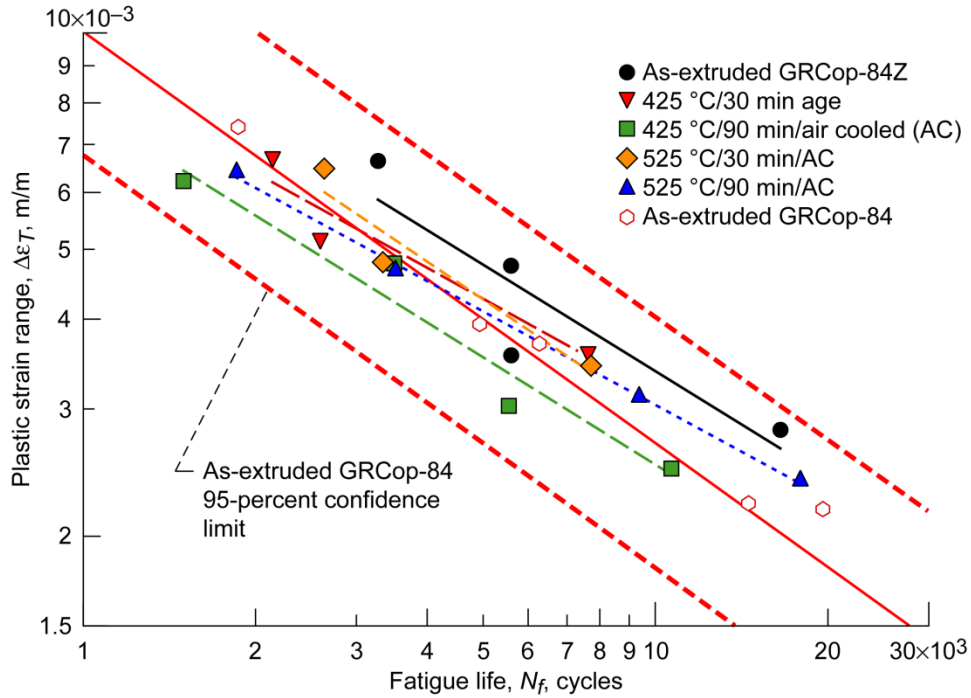
Figure 15.—Fatigue life as a function of plastic strain range.

To determine if there were statistically significant differences between specimens with different heat treatments, the data were fit to Equation (2) with the plastic strain range being used instead of the total strain range. The results of the forward stepwise regression are given in Table X. The analysis indicated that the as-extruded GRCop-84Z has a slightly higher plastic strain range at a given life or a longer life at a given plastic strain. The plastic strain range difference increases as life increases rather than being a constant offset.

Figure 16 shows the cyclic strength at half-life ($\Delta\sigma$) for GRCop-84 and GRCop-84Z as a function of plastic strain range at the half-life of the specimens ($\Delta\varepsilon_P$). The results indicate that GRCop-84Z had a consistently greater strength than GRCop-84 at room temperature. This is consistent with the increase in room temperature strength shown in Figure 6 and Figure 7. A forward stepwise regression analysis using Equation (3) was done to confirm that the strengths were statistically significantly greater. As shown in Table XI, the statistical analysis revealed that, in all heat-treated conditions, the strength of GRCop-84Z was significantly different from the as-extruded GRCop-84 strength. Even the as-received GRCop-84Z specimens had a higher strength, albeit only slightly greater than that of GRCop-84. Furthermore, the differences were a constant offset, indicating that the GRCop-84Z curves had the same slope as the as-received GRCop-84 regression curve.

Following testing the fracture surfaces were examined optically. A typical optical fractography appears in Figure 17. The initiation sites tended to be at the surface or at near-surface imperfections. No changes in the initiation sites were observed between GRCop-84 and GRCop-84Z specimens.

TABLE X.—RESULTS OF FORWARD STEPWISE REGRESSION ANALYSIS
FOR LIFE VERSUS PLASTIC STRAIN RANGE, $\Delta\varepsilon_P$

(a) Goodness of fit.

Multiple correlation coefficient, R	0.988
Coefficient of determination, R^2	.976
Adjusted R^2	.975
Standard error of estimate, $S_{Y.X}$	.0721

(b) Analysis of variance.

Group	Degrees of freedom	Sum of squares	Mean square	F value[a]	Probability
Regression	2	8.044	4.022	773.268	<0.001
Residual	38	0.198	0.00520	----------	--------

(c) Variables in model.

Variable[b]	Coefficient	Standard error	F value[a]	Probability
Constant	−0.304	0.0510	------------	--------
$\log_{10}$(life)	−0.566	0.0145	1533.251	<0.001
$B_1 \log_{10}$(life)	0.0222	0.0101	4.886	0.033

(d) Variables not in model.

Variable[b]	F value[a]	Probability
B_1	0.127	0.723
B_2	.0482	.827
B_3	3.108	.086
B_4	.377	.543
B_5	.306	.584
$B_2 \log_{10}$(life)	.0736	.788
$B_3 \log_{10}$(life)	2.874	.098
$B_4 \log_{10}$(life)	.386	.538
$B_5 \log_{10}$(life)	.495	.486

[a]Value of the F distribution for X degrees of freedom associated with the numerator and Y degrees of freedom associated with the denominator.
[b]B_1 to B_5 are blocking variables indicating treatments that the material received (see Table II).
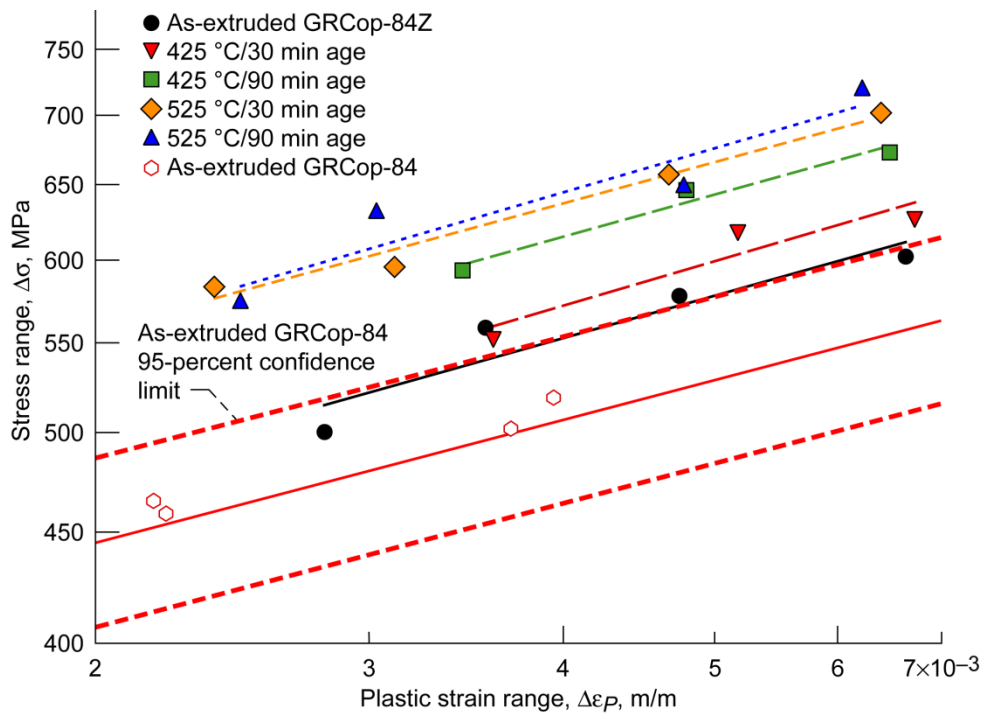
Figure 16.—Cyclic strength as a function of plastic strain range.

TABLE XI.—RESULTS OF FORWARD STEPWISE REGRESSION ANALYSIS
FOR PLASTIC STRAIN RANGE, $\Delta\varepsilon_P$, VERSUS STRESS RANGE, $\Delta\sigma$

(a) Goodness of fit.

Multiple correlation coefficient, R	0.987
Coefficient of determination, R^2	.974
Adjusted R^2	.969
Standard error of estimate, $S_{Y.X}$	.0155

(b) Analysis of variance.

Group	Degrees of freedom	Sum of squares	Mean square	F value[a]	Probability
Regression	6	0.302	0.0504	209.233	<0.001
Residual	34	0.00819	0.000241	----------	--------

(c) Variables in model.

Variable[b]	Coefficient	Standard error	F value[a]	Probability
Constant	3.157	0.0125	------------	-------
$\log_{10}(\sigma)$	.188	.00556	1149.830	<0.001
B_1	.0380	.00849	20.032	<.001
B_2	.0547	.00956	32.740	<.001
B_3	.105	.00852	150.650	<.001
B_4	.0851	.00957	79.096	<.001
B_5	.0994	.00852	136.146	<.001

(d) Variables not in model.

Variable[b]	F value[a]	Probability
$B_1 \log_{10}(\sigma)$	0.0501	0.824
$B_2 \log_{10}(\sigma)$	.0682	.796
$B_3 \log_{10}(\sigma)$	.159	.693
$B_4 \log_{10}(\sigma)$	.0168	.898
$B_5 \log_{10}(\sigma)$	.0188	.892

[a]Value of the F distribution for X degrees of freedom associated with the numerator and Y degrees of freedom associated with the denominator.
[b]B_1 to B_5 are blocking variables indicating the treatment that the material received (see Table II).
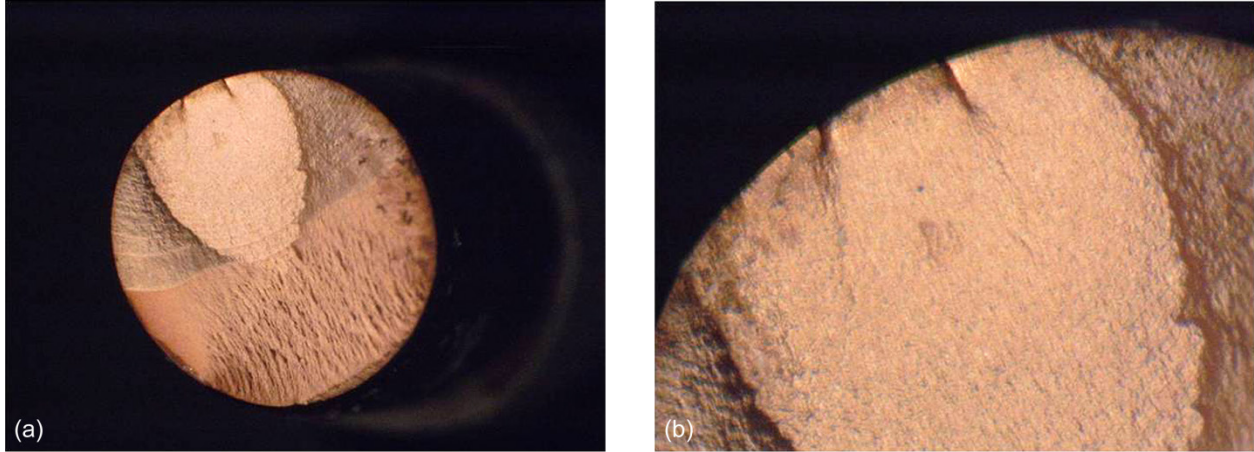
Figure 17.—Typical optical fractograph of GRCop-94Z low cycle fatigue specimen aged at 425 °C/30 min/air cooled. Total strain range, 1.2-percent; life, 2141 cycles. (a) Fracture surface. (b) Detail of fracture initiation site.

4.0   Discussion

A comparison of GRCop-84 and GRCop-84Z revealed several beneficial changes resulting from the addition of Zr. Unfortunately, an increase in LCF life was not one of the observed benefits; though, as discussed later, there may be a benefit at elevated temperatures.

4.1   Tensile Properties

The tensile test data indicate that the addition of 0.4 wt% Zr to GRCop-84 had a beneficial effect relative to the baseline as-extruded GRCop-84 properties. Fairly strong effects in the as-extruded and aged conditions were observed. It had been expected that the benefits would be greatest at room temperature. Significant increases were seen for the aged GRCop-84Z samples with increases in yield strength of 20 percent being achieved for the specimens aged at 525 °C. However, the greatest benefits were seen in specimens tested at 500 °C. The yield strength at 500 °C increased at least 35 percent for the aged GRCop-84Z specimens. Three of the four aging conditions increased the yield strength over 60 percent.

Even the as-extruded GRCop-84Z showed an increase in yield strength, probably because it had a higher total volume fraction of Cr_2Nb and Cu_5Zr precipitates. Cu_5Zr precipitates can act as impenetrable barriers to dislocation movement and provide additional strengthening. The Cu_5Zr precipitates were expected to contribute approximately 2 vol% precipitates on the basis of the composition. That raises the total volume fraction of precipitates to 16 vol%. This represents an increase of 15 percent in the precipitate volume fraction.

If the simplifying assumptions are made that the precipitates are spherical and widely spaced, the Ashby-Orowan equation (Ref. 24) can be expressed as

$$\sigma \cong K\left(\frac{V_f^{1/2}}{r}\right)\ln\left(\frac{r}{b}\right) \qquad (4)$$

Here σ is the yield strength of the material (in megapascals); K is a constant equal to 0.1836 Gb, where G is the shear modulus in megapascals and b is the Burgers vector in the slip direction in nanometers; V_f is the volume fraction of precipitate; and r is the average radius of the precipitates in nanometers. Although

the simplifications may not apply to GRCop-84Z, it is possible to use this equation to estimate order-of-magnitude changes.

According to the Ashby-Orowan model, the increase in volume fraction of precipitates from 14 to 16 vol% alone would increase the strength by 7 percent. Since the Cu_xZr precipitates are finer, the Ashby-Orowan model also predicts a considerable increase in strength from the reduced precipitate size. No quantitative measurements were made of the Cu_xZr precipitate size, but if one uses an estimate of the Cu_xZr precipitate diameter being one-quarter to one-third of the diameter of the Cr_2Nb precipitates and assumes the strengthening of each type of precipitate to be additive, the total strength increase would be on the order of 23 to 39 percent. This estimate for the increase in strength is consistent with the observed difference in the room temperature strengths of GRCop-84 and GRCop-84Z. This indicates that the Cu_5Zr precipitates are acting as expected to provide additional strengthening.

The very large increase in 500 °C strength and ductility was unexpected. It had been assumed that the Cu_5Zr precipitates would start to overage at this test temperature and not contribute such a substantial increase in strength. Instead, they had the greatest effect at this temperature. It appears from the creep data that the beneficial effects persist at this temperature over an extended period of time since creep tests lasting up to approximately 3000 h did not show any clear signs of overaging. It appears that the kinetics of precipitate growth are slow even at this temperature. Additional work will need to be done to determine the maximum temperature at which the Cu_5Zr precipitates will still have a useful effect.

There is an apparent incongruity in the ductility of GRCop-84Z relative to GRCop-84. The ductility of GRCop-84Z as measured by the elongation of the gauge section increased at room temperature. Examination of the samples after testing showed that the reduced section was fairly constant in diameter. Little or no necking or other dimensional instabilities were noted. Apparently the deformation remained uniform for longer than occurred in GRCop-84. This dimensional stability prevented the formation of a neck during tensile testing. Without a pronounced neck, as is typical of GRCop-84 and most other Cu alloys, there was less reduction in area at the fracture site. The failure stress was also higher because the sample still had a large area relative to a sample that undergoes considerable necking. In fact, the fracture strength was only a bit less than the UTS as shown in Figure 10(a). The change to a more uniform deformation throughout the entire gauge section increased the elongation, but the lack of a neck decreased the reduction in area. This gave ambiguous results as to whether or not the addition of Zr improves the ductility. For many applications, the uniform tensile elongation is the more important measure of ductility, and if this criteria is used, the Zr addition was beneficial.

One interesting possible benefit from the lack of necking at room temperature is that GRCop-84Z may prove to be more formable. The uniform nature of the deformation should allow bending and other forming operations to occur without thinning and the potential failure of the part. No work has been performed in this area, but it is a potential area for future study.

The increase in ductility at 500 °C was caused by a combination of more uniform elongation in the reduced gauge length combined with more necking once a dimensional instability appeared. The increase in temperature presumably decreased the shear stress and may have allowed dislocation climb to occur around the Cu_5Zr precipitates. The increase in temperature also could have activated one or more additional slip systems. These changes allowed more shear deformation to occur in the neck region. Because of the shear, the samples could deform more than at room temperature. This resulted in more necking and a larger reduction in area. The increased strength and more uniform deformation allow GRCop-84Z to deform more than GRCop-84, so the reduction in area at 500 °C increased. The large increases in both tensile elongation and reduction in area unambiguously demonstrate that addition of Zr increased the ductility at 500 °C.

One goal of adding Zr to GRCop-84 was to increase the room temperature yield strength by at least 15 percent. This goal was exceeded. Beyond the increase in room temperature yield strength, the Zr addition increased the room temperature UTS and the 500 °C yield strength and UTS while generally improving the ductility. The benefits are substantial, and the addition of Zr clearly improved the tensile properties.

4.2   Creep Properties

The creep data indicate that the addition of Zr has a very strong positive effect on creep properties in aged GRCop-84Z. As shown in Table VII, at 500 °C, samples aged at 425 and 525 °C had their creep rate decreased by a factor of $10^{0.78}$, or 6 times, and their creep life increased by a factor of $10^{0.64}$, or 4.4 times. The fine Cu_5Zr precipitates created during aging act as strong barriers to dislocation movement. The increased yield strength also means that the creep specimens are tested at stresses below the 0.2% offset yield strength, so the amount of macroscopic plastic deformation upon loading is greatly decreased, though not completely eliminated.

The increase in 500 °C ductility does not appear to be a major contributing factor to the improvement in creep life. The as-extruded GRCop-84Z specimens have better ductility than the GRCop-84 specimens, but only the low stress creep tests demonstrated better lives. If increased uniform elongation had been improving creep lives by providing a larger "pool" of ductility and extending the time in steady-state creep, it would be expected that all of the as-extruded GRCop-84Z specimens would exhibit at least some increase in life. This was not observed.

The as-extruded GRCop-84Z showed two distinct regimes in its creep properties. At higher stresses, the material behaved similarly to GRCop-84. This was expected since the material lacked the finer Cu_xZr precipitates created by a solution and aging heat treatment. At the lowest stress tested, the as-extruded GRCop-84Z exhibited much better creep properties than GRCop-84. The as-received specimens' rates and lives approached those of the aged GRCop-84Z specimens. As shown in Table VII, the creep rate decreased by a factor of $10^{0.40}$, or 2.5 times, and the creep life increased by a factor of $10^{0.42}$, or 2.6 times. It appears from this behavior that there is a minimum stress required to overcome the barriers presented by the coarser Cu_xZr precipitates in the as-extruded GRCop-84Z. Most likely, this is a stress associated with dislocation climb or another similar mechanism. Once the minimum stress was achieved and the dislocations could climb or otherwise circumvent the barriers, the as-extruded GRCop-84Z acted similar to the as-extruded GRCop-84. The finer precipitates in the aged GRCop-84Z specimens probably require a higher stress for dislocation climb to become active, or dislocation climb is not active in aged specimens for some unknown reason.

4.3   Low Cycle Fatigue Properties

The addition of Zr to GRCop-84 did not have the beneficial effects on LCF lives anticipated from Figure 1. Instead the LCF specimen lives for all GRCop-84Z heat treatments were generally within the 95-percent confidence limit for GRCop-84. Those that were not within the 95-percent confidence limits were just below the lower confidence limit. The lives tended toward the lower limit when plotted against total strain, but lives based on plastic strain were similar to those for GRCop-84. The cyclic strength of GRCop-84Z did show a definite improvement over GRCop-84, which is consistent with GRCop-84Z's higher strength.

In general, ductility correlates well with the fatigue life of a material as was explained by Coffin and Manson (Ref. 25). Materials with large amounts of ductility can absorb and tolerate large amounts of damage prior to failure. The relative room temperature ductility of GRCop-84Z as measured by the tensile elongation is 3.4 to 29.8 percent greater than that of GRCop-84, but the ductility as measured by the reduction in area is reduced by 23.9 to 45.2 percent. The differing amounts of ductility make it unclear if the room temperature LCF lives of GRCop-84Z should increase or decrease. In both cases, the absolute ductility remained above 15 percent, so GRCop-84Z never became brittle and it still exhibited good LCF lives.

Examination of the fracture ignition sites indicated that cracks generally initiated at the surface. The cracks propagated inwards until they linked up to form a single crack that propagated to eventual failure of the specimen. Some cracks initiated at small surface defects, small inclusions, and pores, as was observed in GRCop-84 LCF fractures. These small defects did not appear to have a strong effect on the LCF lives of GRCop-84 or GRCop-84Z. Rather they were just the sites of the highest local stress

concentration or of a microscopic preexisting crack. Given the similar fracture surface morphologies and behaviors of GRCop-84 and GRCop-84Z, the authors concluded that adding Zr to make GRCop-84Z probably did not change the fracture mechanism or sensitization from that of GRCop-84.

Because of the early termination of the program, the unexpectedly lower lives of GRCop-84Z could not be examined in the level of detail desired. The authors speculate that the area of the GRCop-84Z in the plane perpendicular to the applied load near the crack tips that undergoes plastic deformation is smaller. This is based on the lower macroscopic reduction in area observed for GRCop-84Z during tensile testing. With less material undergoing plastic deformation, damage accumulates quicker and the cracks can propagate more readily. This effect is partially countered by the greater tensile ductility, which increases the amount of material in the direction of the applied load undergoing deformation. The presence of more obstacles in the form of fine Cu_xZr precipitates can also have a beneficial effect both in strengthening the GRCop-84Z and in preventing persistent slip bands. If one assumes that all three mechanisms are operative, the reduction in volume appears to be slightly more influential than the combined effects of greater tensile ductility and more precipitates.

Figure 6 and Figure 7 show that the 0.2% offset tensile yield strength of GRCop-84Z is 2.3 to 20.6 percent greater than for GRCop-84 and that the UTS is 19.9 to 26.8 percent greater. The higher tensile strength is consistent with the higher cyclic strength and indicates that the fine Cu_5Zr precipitates do strengthen GRCop-84Z during fatigue.

As noted in the results for the forward stepwise regression analyses (Table IX and Table X), the 425 °C aging appeared to have a greater effect on the room temperature GRCop-84Z LCF life than the 525 °C aging did. The effects also tended to be negative rather than positive: for example, the LCF life based on total strain (Table IX) was statistically lower than for GRCop-84 and the 525 °C aged GRCop-84Z. This may indicate that a 425 °C aging temperature could have a long-term detrimental effect. Examination of samples given longer aging times is recommended if a combustion chamber liner or other GRCop-84Z part is to be operated in this temperature range.

Although the LCF testing was conducted only at room temperature, some speculation was given to the benefits of Zr on elevated temperature LCF lives and cyclic stresses. As shown in Figure 8, the 500 °C tensile strength of aged GRCop-84Z is much greater than that of GRCop-84. The 0.2% offset yield strength increases 35.6 to 63.5 percent, and the UTS increases 42.9 to 67.6 percent. It is anticipated that this large increase in elevated temperature strength will translate into GRCop-84Z having much greater 500 °C cyclic stresses than GRCop-84.

Unlike the room temperature tests, the 500 °C data show large increases in both the tensile elongation (56.7 to 84.6 percent) and reduction in area (89.7 to 128.0 percent). Assuming that the elevated temperature LCF lives follow the common trend of increased life with increased ductility, the authors believe that the 500 °C LCF lives will show benefits from the addition of Zr to GRCop-84. Unfortunately, this hypothesis could not be tested before the experimental work concluded. The authors hope that additional GRCop-84Z LCF testing at 500 °C can be done in the future.

The forward stepwise regression analyses allow the observed effects of heat treatment and adding Zr to be quantified. For the lives, the statistically significant differences observed mostly show an offset in the response relative to the baseline. This indicates that GRCop-84 and GRCop-84Z probably have the same failure mechanism. It is also consistent with the fractography observations. In the one case where the slope changes, there is only a small difference in slope, which could well be influenced by only having three data points. It is likely that the difference would either disappear or the dependency would change to an offset with additional data for as-received GRCop-84Z.

The regression analysis of the strengths also shows offsets in the curves with the addition of Zr and the various heat treatments. The lack of a change in slope again indicates that the mechanisms operating probably remain the same. The addition of Zr and the formation of fine Cu_5Zr precipitates is probably just additively strengthening GRCop-84Z as expected.

4.4   Aging Temperature and Time

There are clear strength and creep benefits to a solution and aging heat treatment for GRCop-84Z. The as-extruded GRCop-84Z, although it has Cu$_x$Zr precipitates that are finer than most of the Cr$_2$Nb precipitates, does not achieve the property increases of aged GRCop-84Z. The effects of aging are not as unambiguous for the tensile ductility and LCF lives. The authors believe that overall the addition of Zr and the use of a solution and age heat treatment will improve the properties of GRCop-84Z and make them generally superior to those of GRCop-84.

The optimum aging temperature and time were not determined in this study because of the limited material and data available, but the data indicated that both 425 and 525 °C are good choices. Neither appears to overage the Cu$_5$Zr precipitates even after 90 min. The creep data, which extend to 3000 h at 500 °C, also support aging in this temperature range. The creep properties of the aged GRCop-84 specimens do not indicate that the Cu$_x$Zr precipitates undergo overaging even after very extended times at 500 °C. This indicates good stability for the Cu$_x$Zr precipitates and slow growth kinetics. These are desirable traits for a precipitate.

Higher aging temperatures may yield comparable and perhaps better results, but it is more likely that overaging will occur instead. Lower temperatures will require longer times, which are not desirable in a commercial aging process. It appears that the currently used temperatures, if not optimum, are suitable.

Overall, it appears that aging at 425 °C for 90 min gives the best combination of mechanical properties. This temperature is probably a good choice for aging cold-worked GRCop-84Z as well. Applications that require the highest LCF lives and that can tolerate a small decrease in tensile and creep properties may need a 525 °C aging temperature since LCF lives were shown to be slightly decreased by aging at 425 °C. More testing to optimize the aging time and temperature is required, but the preliminary survey shows great promise for aged Cu-Cr-Nb-Zr alloys in the temperature range of this study.

4.5   Cold Rolling

Cold rolling is a major strengthening mechanism. Cu-Cr and Cu-Cr-Zr alloys typically use cold work followed by an aging step to increase their strengths (Refs. 11 and 12). Similar processing with GRCop-84Z had been planned, but time and funding did not permit this work to proceed to the point where quantitative results could be obtained. Some observations do allow speculation as to the benefits that may be obtained by cold working and aging GRCop-84Z.

There are considerable differences between the yield strengths and UTS of the GRCop-84Z samples. GRCop-84Z also has good ductility. Prior work with GRCop-84, which has similar properties, showed that GRCop-84 can be cold rolled 90 percent or more. The authors believe that GRCop-84Z also could be cold rolled extensively. Such rolling should increase at least the room temperature yield strength of GRCop-84Z. This is consistent with the improvements seen in cold-worked Cu-Zr specimens (Ref. 26).

The addition of Zr to Cu-Cr alloys has been shown to retard annealing at 500 °C through the precipitation of Cu$_x$Zr precipitates (Ref. 27). It is likely that the same will happen in GRCop-84Z. Prior work with hard-drawn Cu-0.15 Zr and Cu-1 Cr-0.1 Zr has shown, on the basis of the alloys' retention of high strength, that the cold work is not lost at 500 °C (Refs. 5 and 28). This indicates that the Cu$_x$Zr precipitates are not coarsening or dissolving much at this temperature. If this is also the case for GRCop-84Z, which seems likely from the current results, then the tensile properties up to 500 °C could be improved further by cold working.

At the present time it is unknown how much improvement could be realized, but the yield strength of cold-worked GRCop-84Z is likely to approach that of cold-worked Cu-Zr and Cu-Cr-Zr alloys between room temperature and 500 °C. This will make GRCop-84Z more competitive with these and similar alloys.

5.0   Future Work

The program terminated early with many questions remaining unanswered. The authors suggest that any follow-on work include the following:

1. The thermal and electrical resistivity of GRCop-84Z must be measured to determine if the Zr addition has a negative effect and how large the effect is. The authors believe that the addition of more fine precipitates to act as electron scattering points will decrease the thermal conductivity slightly, but this may be countered to some extent by removing oxygen from the matrix.
2. Cold-worked material must be tested. Cold working is a major strengthening mechanism for competitive alloys. The addition of Zr is expected to retard the recovery and recrystallization so that cold-worked material could be used up to at least 500 °C. The actual point where the benefits of cold work are lost needs to be determined to examine the potential benefits for rocket engine and other applications.
3. The LCF properties at 500 °C must be tested to determine if adding Zr improves LCF properties at elevated temperatures. It was anticipated that the addition of Zr would primarily benefit the alloy at low temperatures, but the unexpected improvements in 500 °C properties indicate that Zr has a larger positive effect at the upper range of the anticipated operating temperatures.
4. The tensile properties of GRCop-84Z should be tested at more temperatures to determine the intermediate tensile properties and at what temperature the benefits of adding Zr cease. Testing at intermediate temperatures will also determine if the unusual changes in the ductility of GRCop-84Z relative to GRCop-84 occur above room temperature.
5. Although the current aging temperatures and times are suitable for most applications, they cannot be considered to be optimized. Tensile testing with additional aging temperatures to determine the optimum temperature for both solution-heat-treated and cold-worked GRCop-84Z may reveal that further benefits can be gained through better heat treatments.

6.0   Summary and Conclusions

It was observed that literature values of mechanical properties for Cu-based alloys increased when small amounts of Zr were added, so a preliminary examination was undertaken to determine if the addition of Zr to GRCop-84 would produce beneficial effects.

The addition of Zr clearly produced changes in the tensile properties of GRCop-84 at both room temperature and 500 °C. At room temperature, the 0.2% offset yield strength was increased between 2.3 and 20.6 percent depending on the aging treatment. The 500 °C yield strength increased even more, with gains between 25.2 and 63.5 percent, again depending on the aging treatment. Similar increases in the ultimate tensile strength and tensile elongations occurred. The reduction in area actually decreased at room temperature because less necking occurred, but it increased 99.7 to 128.0 percent at 500 °C.

The 500 °C creep properties of aged GRCop-84Z showed considerable improvements over GRCop-84. Aged GRCop-84Z samples had a nearly 2-order-of-magnitude decrease in creep rate and over 1-order-of-magnitude increase in creep life in comparison to GRCop-84. Even the unaged, as-extruded GRCop-84Z was superior to GRCop-84 by similar margins at the lowest applied stress tested and equal at higher applied stresses.

The room temperature low cycle fatigue (LCF) lives of GRCop-84Z were generally equal to those of GRCop-84. Only the GRCop-84Z samples aged at 425 °C showed a potential slight decrease in the LCF life relative to GRCop-84, and the difference was probably not of great engineering significance. The stress range for GRCop-84Z exceeded that of GRCop-84 by 50 to 115 MPa depending on the heat treatment. Since LCF lives are generally related to ductility, the authors speculate that the 500 °C LCF lives of GRCop-84Z would exceed those of GRCop-84 since GRCop-84Z has much greater tensile ductility (>50-percent increase in elongation and >95-percent increase in reduction in area). Likewise, the increase in 500 °C strength will probably translate into increased stress ranges at 500 °C.

The addition of Zr to GRCop-84 showed clear benefits in most of the mechanical properties tested. Aging appeared to enhance these benefits. Additional benefits to the mechanical properties should be realized if the material is cold worked prior to testing. Cold working may be required to improve the room temperature mechanical properties to make them competitive with other high-strength, high-conductivity Cu-based alloys. Although most of the benefits of Zr were expected to occur at room temperature, in fact the greatest benefits occurred at 500 °C.

References

1. Esposito, John J.; and Zabora, Ronald F.: Thrust Chamber Life Prediction. NASA CR–134806, vol. 1, 1975.
2. Grant, N.J.; Lee, A.; and Lou, M.: Multiple Hardening Mechanisms for High Strength, High Temperature, High Conductivity Copper Base Alloys. High Conductivity Copper and Aluminum Alloys, Evan Ling and Pierre W. Taubenblat, eds., The Metallurgical Society of AIME, Warrendale, PA, 1984, pp. 103–117.
3. Mollard, F.R.; Wilke, K.G.; and Chaudhry, A.R.: Copper-Beryllium for Elevated Temperature Electronic and Electrical Applications. Evan Ling and Pierre W. Taubenblat, eds., The Metallurgical Society of AIME, Warrendale, PA, 1984, pp. 147–167.
4. Conway, J.B.; Stentz, R.H.; and Berling, J.T.: High Temperature, Low-Cycle Fatigue of Copper-Base Alloys in Argon; Part I—Preliminary Results for 12 Alloys at 1000° F (538° C). NASA CR–121259, 1973.
5. deGroh, Henry C., III; Ellis, David L.; and Loewenthal, William S.: Comparison of GRCop-84 to Other High Thermal Conductive Cu Alloys. NASA/TM—2007-214663, 2007.
6. Arias, D.; and Abriata, J.P.: Cu-Zr (Copper-Zirconium). Phase Diagrams of Binary Copper Alloys, Monograph Series on Alloy Phase Diagrams, Vol. 10, P.R. Subramanian, D.J. Chakrabarti, and D.E. Laughlin, eds., ASM International, Materials Park, OH, 1994, pp. 497–502.
7. Zeng, K.J.; and Hämäläinen, M.: A Theoretical Study of the Phase Equilibria in the Cu-Cr-Zr System. J. Alloys Compd., vol. 220, nos. 1–2, 1995, pp. 53–61.
8. Zeng, K.J.; Hämäläinen, M.; and Lilius, K.: Phase Relationships in Cu-Rich Corner of the Cu-Cr-Zr Phase Diagram. Scr. Metall. Mater., vol. 32, no. 12, 1995, pp. 2009–2014.
9. Ellis, David L.: Observations of a Cast Cu-Cr-Zr Alloy. NASA/TM—2006-213968, 2006.
10. Taubenblat, P.W.; Smith, W.E.; and Graviano, A.R.: Properties and Applications of High Strength, High Conductivity Coppers and Copper Alloys. High Conductivity Copper and Aluminum Alloys, Evan Ling and Pierre W. Taubenblat, eds., The Metallurgical Society of AIME, Warrendale, PA, 1984, pp. 19–30.
11. Callcut, Vin: High Copper Alloys—High Strength Coppers for Demanding Electrical Applications. Copper Development Association, 2006. http://www.copper.org/publications/newsletters/innovations/2006/09/high_cu_alloys.html Accessed February 9, 2011.
12. Application Data Sheet: Mechanical Properties of Copper and Copper Alloys at Low Temperatures. Publist#: 104/5, Copper Development Association, 2011. http://www.copper.org/resources/properties/144_8/144_8.html Accessed February 9, 2011.
13. Kuznetsov, G.M.: Investigation of the Phase Diagram of the Cu-Zr System. Sov. Non-Ferrous Met. Res., vol. 6, 1978, pp. 267–268.
14. Glimois, J.L.; Forey, P.; and Feron, J.L.: Structural and Physical Studies of Copper-Rich Side in the Cu-Zr System. J. Less Common Met., vol. 113, no. 2, 1985, pp. 213–224.
15. Perry, A.J.; and Hugi, W.: Contribution to the Copper-Rich Copper-Zirconium Phase Diagram. J. Inst. Met., vol. 100, 1972, pp. 378–380.
16. Lundin, C.E.; McPherson, D.J.; and Hansen, M.: System Zirconium-Copper. Trans. AIME, vol. 197, 1953, pp. 273–278.

17. Ellis, David L.; and Michal, Gary M.: Precipitation Strengthened High Strength, High Conductivity Cu-Cr-Nb Alloys Produced by Chill Block Melt Spinning. NASA CR–185144, 1989.
18. Standard Test Methods for Tension Testing of Metallic Materials. Book of Standards, ASTM E–8, vol. 03.01, 2009.
19. Ellis, David L.; Loewenthal, William S.; and Haller, Harold: Creep of Commercially Produced GRCop-84. NASA/TM—2012-216998, 2012.
20. Ellis, D.L.: GRCop-84. Aerospace Structural Materials Handbook, Al Gunderson, Stanley J. Setlak, and William F. Brown, Jr., eds., 40th ed., vol. 6, CINDAS, West Lafayette, IN, 2002.
21. Monkman, F.C.; and Grant, N.J.: An Empirical Relationship Between Rupture Life and Minimum Creep Rate in Creep-Rupture Tests. Proc. ASTM, no. 56, 1956, pp. 593–620.
22. Ellis, D.L.; Walley, J.L.; and Ferry, M.H.: The Effects of Processing Upon the Creep Properties of GRCop-84, to be published.
23. Lerch, Bradley A.; Ellis, David L.; and Yun, HeeMan: Low Cycle Fatigue Behavior of GRCop-84. NASA/TM—2010-216737, 2010. Available from the Center for Aerospace Information.
24. Ashby, M.F.: The Theory of the Critical Shear Stress and Work Hardening of Dispersion-Hardened Crystals. Oxide Dispersion Strengthening, Proceedings of Metallurgical Society Conferences, vol. 47, New York, NY, 1968, p. 143.
25. Meyers, Marc André; and Chawla, Krishan Kumar: Mechanical Metallurgy: Principles and Applications. Prentice-Hall, Inc., Englewood Cliffs, NJ, 1984, Sec. 21.1.4, Fatigue Strength or Fatigue Life, pp. 695–699.
26. Horn, D.D.; and Lewis, H.F.: Property Investigation of Copper Base Alloys at Ambient and Elevated Temperatures. AEDC–TR–65–72, 1965.
27. Su, J.H., et al.: Recrystallization and Precipitation Behavior of Cu-Cr-Zr Alloy. J. Mater. Eng. Perform., vol. 16, no. 4, 2007, pp. 490–493.
28. de Groh, H.C.; Ellis, D.L.; and Loewenthal, W.S.: Comparison of GRCop-84 to Other Cu Alloys With High Thermal Conductivities. J. Mater. Eng. Perform., vol. 17, no. 4, 2008, pp. 594–606.

REPORT DOCUMENTATION PAGE		*Form Approved* *OMB No. 0704-0188*
The public reporting burden for this collection of information is estimated to average 1 hour per response, including the time for reviewing instructions, searching existing data sources, gathering and maintaining the data needed, and completing and reviewing the collection of information. Send comments regarding this burden estimate or any other aspect of this collection of information, including suggestions for reducing this burden, to Department of Defense, Washington Headquarters Services, Directorate for Information Operations and Reports (0704-0188), 1215 Jefferson Davis Highway, Suite 1204, Arlington, VA 22202-4302. Respondents should be aware that notwithstanding any other provision of law, no person shall be subject to any penalty for failing to comply with a collection of information if it does not display a currently valid OMB control number. **PLEASE DO NOT RETURN YOUR FORM TO THE ABOVE ADDRESS.**		

1. REPORT DATE *(DD-MM-YYYY)* 01-06-2012	**2. REPORT TYPE** Technical Memorandum	**3. DATES COVERED** *(From - To)*	
4. TITLE AND SUBTITLE Improvement of GRCop-84 Through the Addition of Zirconium		**5a. CONTRACT NUMBER**	
		5b. GRANT NUMBER	
		5c. PROGRAM ELEMENT NUMBER	
6. AUTHOR(S) Ellis, David, L.; Lerch, Bradley, A.		**5d. PROJECT NUMBER**	
		5e. TASK NUMBER	
		5f. WORK UNIT NUMBER WBS 463169.04.03.05.01	
7. PERFORMING ORGANIZATION NAME(S) AND ADDRESS(ES) National Aeronautics and Space Administration John H. Glenn Research Center at Lewis Field Cleveland, Ohio 44135-3191		**8. PERFORMING ORGANIZATION REPORT NUMBER** E-17626	
9. SPONSORING/MONITORING AGENCY NAME(S) AND ADDRESS(ES) National Aeronautics and Space Administration Washington, DC 20546-0001		**10. SPONSORING/MONITOR'S ACRONYM(S)** NASA	
		11. SPONSORING/MONITORING REPORT NUMBER NASA/TM-2012-216985	
12. DISTRIBUTION/AVAILABILITY STATEMENT Unclassified-Unlimited Subject Category: 26 Available electronically at http://www.sti.nasa.gov This publication is available from the NASA Center for AeroSpace Information, 443-757-5802			
13. SUPPLEMENTARY NOTES			

14. ABSTRACT
GRCop-84 (Cu-8 at.% Cr-4 at.% Nb) has excellent strength, creep resistance, low cycle fatigue (LCF) life and stability at elevated temperatures. It suffers in comparison to many commercially available precipitation-strengthened alloys below 500 °C (932 °F). It was observed that the addition of Zr consistently improved the mechanical properties of Cu-based alloys especially below 500 °C. In an effort to improve the low temperature properties of GRCop-84, 0.35 wt.% Zr was added to the alloy. Limited tensile, creep, and LCF testing was conducted to determine if improvements occur. The results showed some dramatic increases in the tensile and creep properties at the conditions tested with the probability of additional improvements being possible through cold working. LCF testing at room temperature did not show an improvement, but improvements might occur at elevated temperatures.

15. SUBJECT TERMS
Copper alloys; Mechanical properties

16. SECURITY CLASSIFICATION OF:			**17. LIMITATION OF ABSTRACT**	**18. NUMBER OF PAGES**	**19a. NAME OF RESPONSIBLE PERSON** STI Help Desk (email:help@sti.nasa.gov)
a. REPORT U	**b. ABSTRACT** U	**c. THIS PAGE** U	UU	42	**19b. TELEPHONE NUMBER** *(include area code)* 443-757-5802

Standard Form 298 (Rev. 8-98)
Prescribed by ANSI Std. Z39-18